MOLECULAR AND CELLULAR BIOLOGY, Dec. 2004, p. 10905–10922 Vol. 24, No. 24
0270-7306/04/$08.00+0 DOI: 10.1128/MCB.24.24.10905–10922.2004

Abi2-Deficient Mice Exhibit Defective Cell Migration, Aberrant Dendritic Spine Morphogenesis, and Deficits in Learning and Memory

Matthew Grove,[1] Galina Demyanenko,[2] Asier Echarri,[1] Patricia A. Zipfel,[1] Marisol E. Quiroz,[1] Ramona M. Rodriguiz,[3] Martin Playford,[1] Shelby A. Martensen,[1] Matthew R. Robinson,[1] William C. Wetsel,[3] Patricia F. Maness,[2] and Ann Marie Pendergast[1]*

Department of Pharmacology and Cancer Biology[1] and Departments of Psychiatry, Medicine (Endocrinology), and Cell Biology, Mouse Behavioral and Neuroendocrine Analysis Core Facility,[3] Duke University Medical Center, Durham, and Department of Biochemistry and Biophysics, University of North Carolina School of Medicine, Chapel Hill,[2] North Carolina

Received 4 June 2004/Returned for modification 14 July 2004/Accepted 14 September 2004

The Abl-interactor (Abi) family of adaptor proteins has been linked to signaling pathways involving the Abl tyrosine kinases and the Rac GTPase. Abi proteins localize to sites of actin polymerization in protrusive membrane structures and regulate actin dynamics in vitro. Here we demonstrate that Abi2 modulates cell morphogenesis and migration in vivo. Homozygous deletion of murine *abi2* produced abnormal phenotypes in the eye and brain, the tissues with the highest Abi2 expression. In the absence of Abi2, secondary lens fiber orientation and migration were defective in the eye, without detectable defects in proliferation, differentiation, or apoptosis. These phenotypes were consistent with the localization of Abi2 at adherens junctions in the developing lens and at nascent epithelial cell adherens junctions in vitro. Downregulation of Abi expression by RNA interference impaired adherens junction formation and correlated with downregulation of the Wave actin-nucleation promoting factor. Loss of Abi2 also resulted in cell migration defects in the neocortex and hippocampus, abnormal dendritic spine morphology and density, and severe deficits in short- and long-term memory. These findings support a role for Abi2 in the regulation of cytoskeletal dynamics at adherens junctions and dendritic spines, which is critical for intercellular connectivity, cell morphogenesis, and cognitive functions.

Dynamic regulation of the actin cytoskeleton is required for changes in cell shape, adhesion, migration, and polarization during morphogenesis (54). Specifically, coordinated changes in migration and intercellular adhesion require de novo actin polymerization, a process driven by at least two distinct classes of actin nucleator proteins, the Arp2/3 complex and the formins (71, 73). Actin nucleation through the Arp2/3 complex produces branched actin networks that drive lamellipodia (14, 19, 73). Recently, formins have been shown to nucleate linear, unbranched actin filaments (71). Epithelial cell-cell adhesion has been linked to both Arp2/3 and formin actin nucleator proteins (29, 30).

Actin polymerization provides the driving force for the formation of adherens junctions (69). Adherens junctions are circumferential structures formed during epithelial morphogenesis that connect intercellular contacts at the cell surface to the actin cytoskeleton (54). The assembly of adherens junctions is dependent on the cadherins, a family of transmembrane proteins that mediate calcium-dependent homophilic interactions between adjacent cells. Cadherins are linked to the actin cytoskeleton by α- and β-catenins, and cadherin engagement leads to activation of Rho family GTPases, which are critical regulators of the actin cytoskeleton (16, 54, 77). Rho GTPases localize to sites of cadherin-mediated cell-cell contact and, conversely, cadherin recruitment to sites of intercellular adhesion is disrupted in some cells expressing mutant forms of the Rho family GTPases (18, 77). The Rho family proteins Rac1, Cdc42, RhoA, and RhoC have all been shown to affect adherens junctions in different cell types (18, 51). Activation of the Rac and Cdc42 GTPases is important for the assembly of actin-dependent membrane protrusions in the form of lamellipodia and filopodia, respectively (16). Formation of lamellipodia by activated Rac depends on the WAVE proteins, which stimulate the actin nucleating activity of the Arp2/3 complex (73). Assembly of cadherin-dependent intercellular adhesions can be driven by lamellipodial or filopodial membrane protrusions (14, 19, 30, 69). Among the GTPases, Rac is consistently activated by cadherin adhesion and is preferentially recruited at new cell-cell contacts, where its accumulation correlates with enhanced lamellipodia activity (14, 77). Thus, Rac activation and downstream signaling may coordinate cadherin engagement to actin reorganization at sites of cell-cell adhesion. However, the mechanisms that link Rac activation to actin polymerization during intercellular adhesion are currently unknown. Moreover, the intracellular proteins involved in the regulation of actin reorganization in vivo during epithelial morphogenesis are just beginning to be identified.

Modulation of actin dynamics is also critical for the formation, maturation, and maintenance of dendritic spines (33). Spines are highly dynamic structures that are rich in actin and undergo changes in shape, size, and number during development and are remodeled in an activity-dependent manner in adulthood (79). Abnormal spine density and morphology have

* Corresponding author. Mailing address: Duke University Medical Center, Department of Pharmacology and Cancer Biology, Box 3813, Durham, NC 27710. Phone: (919) 681-8086. Fax: (919) 681-7148. E-mail: pende014@mc.duke.edu.

been associated with neurological disorders such as mental retardation and epilepsy (5). Proteins that regulate the actin cytoskeleton are prime candidates for controlling dendritic spine morphogenesis and synapse formation. Indeed, in vitro studies have shown that Rho, Rac, and Cdc42 modulate dendritic spine shape and number (27, 41). Rac activity, in particular, is important for the maintenance of spine density (41), and regulation of Rho family GTPase signaling has been shown to be critical for normal cognitive functions (46). Dendritic spine formation and maintenance are regulated by glutamate receptors and cell adhesion receptors, such as the cadherins and Eph receptors (15, 23, 33, 40, 43, 68). The mechanisms that link activation of these cell surface receptors to regulation of actin dynamics remain to be defined but may involve regulation of the Rac and Cdc42 GTPases through activation of specific guanine nucleotide exchange factors (GEFs) (27, 43).

Here we identify the Abi2 protein as a component of sites of dynamic actin cytoskeleton remodeling at epithelial cell-cell junctions and dendritic spines. The Abi proteins were initially identified as binding partners for the c-Abl tyrosine kinase (10, 58). The Abi protein family is currently comprised of mammalian Abi1, Abi2, and NESH/Abi3, *Drosophila melanogaster* Abi, *Xenopus laevis* Xlan4, *Dictyostelium discoideum* Abi, and *Caenorhabditis elegan*s Abi (4, 10, 12, 28, 36, 47, 58). In addition to c-Abl, Abi proteins were subsequently shown to interact with the Arg tyrosine kinase, the adaptor protein Eps8, spectrin, the Sos GEF, Nckα/Grb4, Mena, WAVE, and the WAVE-associated Nap1/Nap125 protein (3, 9, 12, 17, 26, 56, 67, 72, 75, 82). Abi proteins share several conserved domains, including SH3, homeodomain homologous region, SNARE, and the WAVE-binding domain (10, 12, 58, 63). Abi1 has been linked to Rac signaling in a trimeric complex that contains Abi1 (also designated E3b1), Eps8, and the Sos GEF. This complex exhibits GEF activity towards the Rac GTPase (56). Overexpression of Abi1 can activate Rac in an Eps8-dependent manner (25), and downregulation of Abi1 function by RNA interference or specific antibodies inhibits Rac-dependent or platelet-derived growth factor-induced membrane ruffling, respectively (26, 56). A similar inhibition of the membrane ruffling response to platelet-derived growth factor stimulation is observed in mouse embryo fibroblasts (MEFs) isolated from c-Abl or Eps8 knockout mice (45, 56). Thus, Abi1 may function in concert with Eps8 or c-Abl to transduce signals from activated growth factor receptors to cytoskeletal reorganization.

Abi1 and Abi2 were purified from brain lysates in protein complexes containing WAVE proteins (13, 59). In vitro studies with purified components showed that WAVE1 is inhibited by a protein complex containing Abi2, Nap1/Nap125, PIR121/Sra1, and HSPC300 and that addition of purified active Rac releases WAVE1 from inhibition, leading to WAVE1-dependent actin polymerization through the Arp2/3 complex (13). However, recent studies showed that Abi and other components of the WAVE complex are required for the formation of lamellipodial protrusions in *Drosophila* and mammalian cells in culture (26, 31, 50, 62). Abi1 positively regulates WAVE stability and localization to the lamellipodia in mammalian cells (12, 26).

Here we demonstrate that homozygous deletion of the murine *abi2* gene results in cell morphogenesis defects in the eye lens and dendritic spines. Loss of *abi2* results in defective orientation and migration of secondary lens fibers, abnormal neuronal migration in the neocortex and hippocampus, aberrant dendritic spine morphology and density, and profound deficits in learning and memory. We show for the first time that Abi2 accumulates at epithelial cell-cell junctions in vitro and in vivo and that downregulation of Abi proteins impairs adherens junction formation. Together, these findings support a role for Abi2 in the regulation of actin dynamics at sites of membrane protrusion in vivo and in vitro.

MATERIALS AND METHODS

Generation of Abi2 knockout mice. A 0.9-kbp noncoding region of the mouse *abi2* genomic locus was isolated from a 129Sv mouse genomic DNA library in Lambda dash II and was used to probe a 129Sv mouse genomic DNA BAC library (Research Genetics). A BAC clone containing the entire *abi2* gene was obtained, and a ~3-kbp genomic region containing exons 2 and 3 was targeted for deletion. The long arm of the targeting construct was an 8.5-kbp HindIII genomic fragment containing exon 5 and beginning immediately downstream of exon 3. Prior to cloning into the targeting vector (pPGKneobpAlox2PGKDTA), this fragment was modified by introduction of stop codons in all three reading frames, and of SacI, XbaI, and SphI restriction sites, into the EcoNI site in exon 5, which destroyed the EcoNI site. To construct the short arm of the targeting construct, a 1,160-bp genomic fragment encoding sequences immediately upstream of exon 2 was amplified by PCR, using 5′ and 3′ primers containing NotI and Bsp120I restriction sites, respectively. This fragment was cloned into the unique NotI site in the targeting vector, thereby destroying the NotI site downstream of the short arm and allowing linearization of the targeting construct with NotI. The linearized construct was electroporated into embryonic stem (ES) cells, and G418-resistant clones were analyzed by PCR using a 3′ primer specific for the neomycin resistance gene and a 5′ primer from the genomic region upstream of the 5′ end of the short arm. Confirmation of PCR-positive clones was done by Southern blotting after digestion of genomic DNA with either SphI (external probe) or EcoNI (internal probe). SphI generated bands of 7.5 and 5 kbp and EcoNI generated bands of 2.8 and 3.5 kbp for the wild-type and targeted alleles, respectively. Correctly targeted ES cells were injected into inbred C57BL/6 blastocysts. Chimeric male mice were bred with wild-type inbred C57BL/6 females, and two F_1 lines were obtained that contained the correctly targeted Abi2 allele. Routine genotyping was carried out by PCR. Mice were backcrossed to the C57BL/6 strain, and F_5 to F_7 offspring were used for analyses.

Plasmids. The *Abi2B* cDNA was cloned into the BamHI site of the *pLEGFP-C1* retroviral vector (Clontech). Constructs were sequenced prior to use.

Cell culture. Primary MEFs were obtained from embryonic day 13.5 (E13.5) embryos and were immortalized using a standard 3T3 protocol. MEF, MDCK, HeLa, and 293T cells were grown in Dulbecco's modified Eagle's medium with 10% fetal bovine serum. For cell-cell junction formation and cell spreading assays, 10^5 MDCK cells were plated onto glass coverslips precoated with collagen IV (Gibco). Primary neurons, obtained from E17.5 cortex or postnatal day 2 (P2) hippocampus, were plated on glass coverslips coated with poly(D-lysine) (100 μg/ml)–laminin (10 μg/ml) or poly(D-lysine) (1 mg/ml), respectively. Cells were grown in neurobasal medium containing B27 supplement, Glutamax, and 1 μg of gentamicin (Gibco)/ml.

Cell transfection and infection. 293T cells were transfected using a standard calcium phosphate method. Infection of MDCK cells was essentially as described elsewhere (48). Briefly, 293T cells were cotransfected with plasmids encoding *gag-pol*, vesicular stomatitis virus G glycoprotein (48), and the *pLEGFP* retroviral vector alone or the *pLEGFP-Abi2B* construct. The virus-containing medium was supplemented with 4 μg of Polybrene (Sigma)/ml, filtered through 0.45-μm-pore-size filters, and used to infect MDCK cells. Two days postinfection, MDCK cells were sorted by fluorescence-activated cell sorting (FACS). Small interfering RNAs (siRNAs) were transfected using Oligofectamine (Invitrogen). Synthetic siRNAs (Dharmacon) for human Abi2B spanned nucleotides 387 to 405 (Abi2.1) or 495 to 513 (Abi2.2), and the siRNA (Dharmacon) for human Abi1 spanned nucleotides 169 to 187.

Antibodies. The anti-Abi2 (5421) and anti-Abi1 (6987) rabbit polyclonal antibodies have been previously described (8). Other antibodies used were the following: mouse monoclonal antibodies anti-α-catenin and anti-β-catenin (Transduction Laboratories), anti-E-cadherin 3G8 (gift from W. James Nelson, Stanford University), anti-WAVE1 (Transduction Laboratories), anti-α tubulin (Sigma), and antibromodeoxyuridine (anti-BrdU; Becton Dickinson), as well as

Cy2 donkey anti-mouse, Cy3 donkey anti-rabbit, donkey anti-mouse, and fluorescein isothiocyanate-conjugated donkey anti-rabbit (Jackson Immunoresearch). The anti-p34Arc rabbit polyclonal antibody was a gift from Matthew Welch (University of California—Berkeley), and the anti-MIP26 and anti-γ-crystallin rabbit polyclonal antibodies were gifts from Sam Zigler (National Eye Institute).

BrdU labeling of mouse embryos. To detect proliferating cells in the eye, 16.5-day timed-pregnant females were injected with BrdU as described previously (39). After 1 h, mice were sacrificed and embryos were removed, genotyped, and embedded in paraffin.

Immunofluorescence. Cells were fixed for 15 min (MDCK) or 10 min (HeLa) with 4% paraformaldehyde (PFA) in phosphate-buffered saline (PBS; pH 7.4) and permeabilized in 0.5% Triton–PBS (MDCK) or 0.2% Triton–PBS (HeLa). Cells were blocked in 10% normal donkey serum–PBS. Primary antibody concentrations were as follows: 0.2 μg of anti-Abi2 (purified)/ml; 0.8 μg of anti-α-catenin/ml; and 0.5 μg of anti-p34 Arc/ml. Cy2 donkey anti-mouse was used at 1/50, Cy3 donkey anti-rabbit was used at 1/200, Cy3 donkey anti-mouse was used at 1/1,500, and Cy2 donkey anti-rabbit was used at 1/400. For staining of F-actin, Alexa 488 phalloidin (Molecular Probes) was diluted to 30 μg/ml in 1% bovine serum albumin–PBS and added to permeabilized cells for 45 min. Stained cells were mounted using Permount (Molecular Probes) and visualized by confocal microscopy. For immunohistochemistry of 5-μm paraffin tissue sections, BrdU-labeled sections were processed as described elsewhere (39) and incubated with anti-BrdU sera. Unlabeled tissue sections were prepared for staining with anti-MIP26 or anti-crystallin antibodies as described elsewhere (39), except that treatment with 2 M HCl was omitted. Antibody staining was visualized with the ABC complex (Vector Systems), and sections were counterstained with methyl green. For tissue staining of frozen 10- to 20-μm cryostat sections, fixation was carried out with 4% PFA for 20 min and the samples were then processed for immunofluorescence or immunohistochemistry. For the latter, endogenous peroxidase was quenched by treatment with 1% hydrogen peroxide for 5 min. Primary neurons were fixed for 15 min with 4% PFA and 4% sucrose in PBS and then processed for immunofluorescence and visualized by confocal microscopy. For tissue staining of frozen 10- to 20-μm cryostat sections, fixation was carried out with 4% PFA for 20 min; the samples were then processed for immunofluorescence or immunohistochemistry. For the latter, endogenous peroxidase was quenched by treatment with 1% hydrogen peroxide for 5 min.

Time-lapse microscopy. MCDK cells stably expressing green fluorescent protein (GFP)-Abi2B were plated on collagen IV-coated plates. The following day, cells were treated with 4 mM EGTA for 30 min to disrupt intercellular adhesion and, after replacing the medium with L-15 medium containing 10% serum, formation of new cell-cell contacts was recorded by using a confocal microscope. Images were taken approximately every 5 to 7 min and were processed with MetaMorph software (Universal imaging).

Cell and tissue lysis and immunoblotting. MDCK cells were lysed in Triton buffer (1% Triton X-100, 150 mM NaCl, 50 mM Tris; pH 7.5) plus inhibitors (1 mM phenylmethylsulfonyl fluoride, 2 mM sodium pyrophosphate, 1 mM sodium orthovanadate, and 1 μg each of leupeptin, aprotinin, and pepstatin A/ml). MEFs were lysed in NP-40 lysis buffer (0.5% NP-40, 50 mM Tris [pH 7.5], 150 mM NaCl, 10% glycerol) with the inhibitors listed above. Lysates were clarified by microcentrifugation (Beckman) at 16,000 × *g* for 20 min. For brain lysates, whole brains were removed by microdissection, placed in TRIzol reagent (Gibco), and homogenized with a Brinkman Polytron 3000 homogenizer. Protein was resuspended in 1% sodium dodecyl sulfate (SDS). Lens lysates were prepared following lens isolation by microdissection. Lenses were homogenized in hypotonic buffer (39). The homogenate was clarified by microcentrifugation at 14,000 rpm, and the supernatant was removed. The resulting insoluble pellet was homogenized in CSK buffer [50 mM NaCl, 10 mM piperazine-N,N′-bis(2-ethanesulfonic acid) (pH 6.8), 3 mM $MgCl_2$, 0.5% Triton X-100, 30 mM sucrose] to extract noncytoskeletal proteins and centrifuged again. Following removal of the supernatant, the pellet was homogenized in RIPA buffer (0.5 M NaCl, 1% NP-40, 0.5% sodium deoxycholate, 0.1% SDS, 50 mM Tris; pH 8.0) and centrifuged. After removal of supernatant (RIPA-soluble fraction), the pellet was resuspended in 2× sample buffer and boiled. Total protein was separated by SDS-polyacrylamide gel electrophoresis (SDS-PAGE) and subjected to Western blotting with the indicated antibodies. Anti-Abi1 and anti-Abi2 sera were diluted 1/1,000. The concentrations employed for primary antibodies were as follows: anti-WAVE1 (0.25 μg/ml), anti-α-catenin (0.25 μg/ml), anti-β-catenin (0.25 μg/ml), and anti-α-tubulin (0.1 μg/ml). Samples used for blotting with the anti-MIP26 antibody were not boiled prior to SDS-PAGE, as described previously (39).

Brain histology and dendritic morphology analyses. Nissl staining and measurements of brains of E18.5 mice and 2- to 3-month-old adult mice were performed as described previously (11). For analyses of dendritic spines, brains from three wild-type and three age-matched $Abi2^{-/-}$ adult mice were impregnated according to the Golgi procedure (55). Briefly, mice were perfused with 10% formalin, and brains were fixed in additional 10% formalin, postfixed in 2.5% potassium dichromate, impregnated with 2% silver nitrate, cut at 150 μm with a Vibratome, dehydrated in ethanol, and embedded in Permount. Spine number was quantified directly with a 40× objective. Fully impregnated layer III and V pyramidal neurons from the somatosensory cortex and pyramidal neurons from the CA1 region of the hippocampus were selected for analysis. Spine density was obtained in different lengths of side branches from apical dendrites in layer V and the CA1 region and from basal dendrites in layer III (10 to 25 segments, with lengths of 10 to 160 μm). Data obtained for wild-type and $Abi2^{-/-}$ mice were compared by a Student's *t* test analysis (two-tailed $P < 0.05$).

Behavioral tests. Experiments were performed using F_5 or F_7 offspring bred to C57BL/6 mice, and results obtained were the same for the F_5 and F_7 offspring. Initial neurophysiological and visual screens to assess gross appearance as well as rudimentary sensory, motor, and visual functions were conducted as described elsewhere (49). Since the Abi2 null mice showed abnormalities in lens development, pupillary responses were evaluated. A 1.13-W halogen prefocused penlight (Brinkmann, Westbury, N.Y.) was aimed into the pupil of the eye for 3 s. This test was repeated three times for each mouse with a 5-s interval between each trial. Tests were videotaped, and digitized videos were scored frame by frame for the absence or presence of the response. These and the neurophysiological data were analyzed by χ^2 tests. To determine whether the mice could visually track a moving object, animals were placed into a circular arena (25 cm in diameter by 28 cm high) and acclimated for 2 min. Animals were presented with a black and white patterned infant feeding spoon that was moved at the eye level along the inside perimeter of the arena over 12 s. Each second was scored for orientation towards the object over 10 trials. Orientations included looking at or fixating on the object, sniffing, grabbing, or biting the moving object or rapidly withdrawing from the moving object accompanied by turning and watching the object approach. To ascertain whether the mice could discriminate a dark from light environment, animals were individually placed into the illuminated half of a passive avoidance chamber (Med Associates, St. Albans, Vt.) with free access to the light and dark chambers for 5 min. The latency to enter the dark chamber and the time spent in each chamber were measured. To examine rudimentary learning and memory, another group of animals was tested in passive avoidance. Mice were placed into the illuminated side, the door was opened to the darkened chamber after 5 s, and the latency to enter the darkened chamber was recorded (all four paws within the darkened compartment). Upon entering the chamber, the door was closed, and after a 10-s interval, the mouse was administered three 2-s scrambled foot shocks (0.4 mA), each separated by a 30-s interval. Performance was evaluated at 30 min, 1 h, or 24 h later. Mice that did not cross within 5 min were removed from the chamber, and the latency was recorded as 300 s. The visual orientation, dark-light discrimination, and passive avoidance data were subjected to analysis of variance tests and Bonferroni a posteriori comparisons. To determine whether multiple exposures to training would improve performance, mice that were originally tested after 1 h were retrained and retested 1 week later (final test). Retention was assessed 1 h after training. To evaluate sensitivity to scrambled foot shock, mice were acclimated to a single chamber for 60 s. Animals were then randomly presented with six different intensities (0.05, 0.1, 0.15, 0.2, 0.3, and 0.4 mA) of 2-s scrambled foot shock. Behavioral responses to the shock were scored using the Observer program (Noldus Information Technology, Leesburg, Va.). The lowest level of response that involved the continuation of activity was scored as 0. Other scoring was as follows: score 1 (low-level response), freezing, face wiping or self-grooming, shaking, or rapid forward departures; score 2 (moderate), retreating from shock or tail rattling; score 3, stationary reactive responses, including kicking and vocalization; score 4, locomotor reactivity, such as darting and leaping; score 5, jumping against walls or the ceiling of the chamber. Behavioral scores were summed for each animal and analyzed as a function of genotype and shock intensity.

RESULTS

Generation of Abi2 null mice. To determine whether Abi2 has a role in regulation of the cytoskeleton and other cellular processes, the *abi2* gene was targeted for deletion in mice (Fig. 1A). Following electroporation of the targeting construct into ES cells, two distinct clones were obtained that contributed to the germ line in founder chimeric mice and were used to produce Abi2 heterozygous mice. The mice were genotyped by Southern blotting (Fig. 1B). Abi2 heterozygous mice were bred

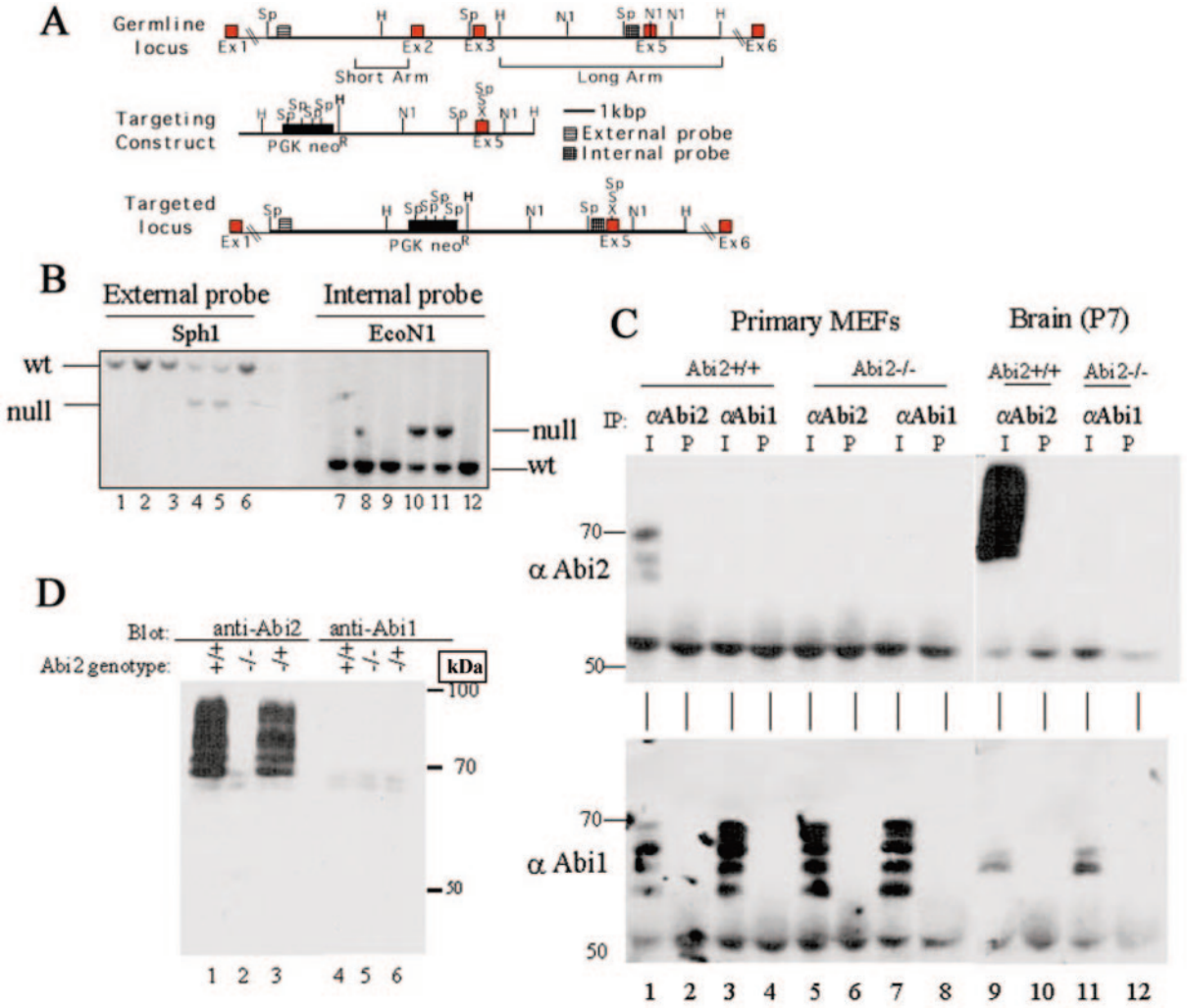

FIG. 1. Generation of Abi2-deficient mice. (A) Targeted disruption of the *abi2* locus. A BAC clone encoding the entire mouse *abi2* gene was used to create a targeting construct in which the PGK-neo cassette replaced the genomic region encompassing exons 2 and 3 of *abi2*. Stop codons were introduced downstream of two Kozak sequences present in exon 5 to prevent the production of truncated Abi2 proteins. Ex, exon; H, HindIII; N1, EcoNI; Sp, SphI; S, SacI; X, XbaI. (B) Southern blot analysis of genomic DNA from wild-type (lanes 1 to 3, 6, 7 to 9, and 12) and Abi2 heterozygous (lanes 4, 5, 10, and 11) mice. Duplicate genomic DNA samples were digested with either SphI or EcoNI and probed with external or internal probes, respectively. An external probe was used to verify targeting, and an internal probe was used to verify the presence of stop codons introduced into exon 5. Bands of the expected size for the genomic locus (wt) and the targeted allele (null) were obtained. (C and D) Analysis of Abi1 and Abi2 protein levels in primary MEFs and brain from Abi2 wild-type (+/+), heterozygous (+/−), and null (−/−) mice. (C) Total protein (500 μg) was immunoprecipitated from primary MEFs (lanes 1 to 8) or P7 brain (lanes 9 to 12) with anti-Abi1 or anti-Abi2 sera (I) or their corresponding preimmune sera (P); the immunoprecipitates were blotted for Abi2 (top) and Abi1 (bottom). The protein band above 50 kDa is the immunoglobulin G heavy chain. (D) Total protein (20 μg) from P7 brain was analyzed by SDS-PAGE and Western blotting for anti-Abi2 (lanes 1 to 3) or anti-Abi1 (lanes 4 to 6). Blots were exposed for equivalent times. Molecular mass standards are shown.

to produce Abi2 null mice, which were viable and fertile and were produced in the expected numbers. Cells and tissues from Abi2 null mice were analyzed to confirm the absence of Abi2 protein. Because transcripts for the related *abi1* are coexpressed with *abi2* transcripts in brain and multiple tissues (8, 10, 58), we examined whether Abi1 protein levels were altered in the absence of Abi2. Polyclonal antibodies against Abi1 (6987) and Abi2 (5421) (8) were employed. The 6987 antibody uniquely recognizes Abi1, while the 5421 antibody primarily recognizes Abi2 and some Abi1 isoforms (Fig. 1 and unpublished data). Analysis of anti-Abi2 immunoprecipitates of MEF lysates from wild-type and Abi2 null embryos showed that Abi2 was completely absent in Abi2 null MEFs (Fig. 1C, upper panel, lanes 1 to 8). Stripping and reprobing of the blot with the anti-Abi1 antibody showed similar levels of Abi1 in the presence or absence of Abi2 (Fig. 1C, lower panel, lanes 1 to 8). Immunoprecipitation of equal amounts of protein from lysates of wild-type mouse brain or MEFs revealed that Abi2 protein was present at relatively high levels in early postnatal brain compared to MEFs, while the reverse was observed for Abi1 (Fig. 1C, compare lanes 1 and 9 in the upper panel to lanes 3 and 11 in the lower panel). Abi2 protein was detected as multiple bands in blots of lysates from wild-type brain, all of which were reduced in Abi2 heterozygotes and were absent in the Abi2 null brain (Fig. 1D, lanes 1 to 3). The multiple Abi2-immunoreactive bands likely correspond to splice variants (un-

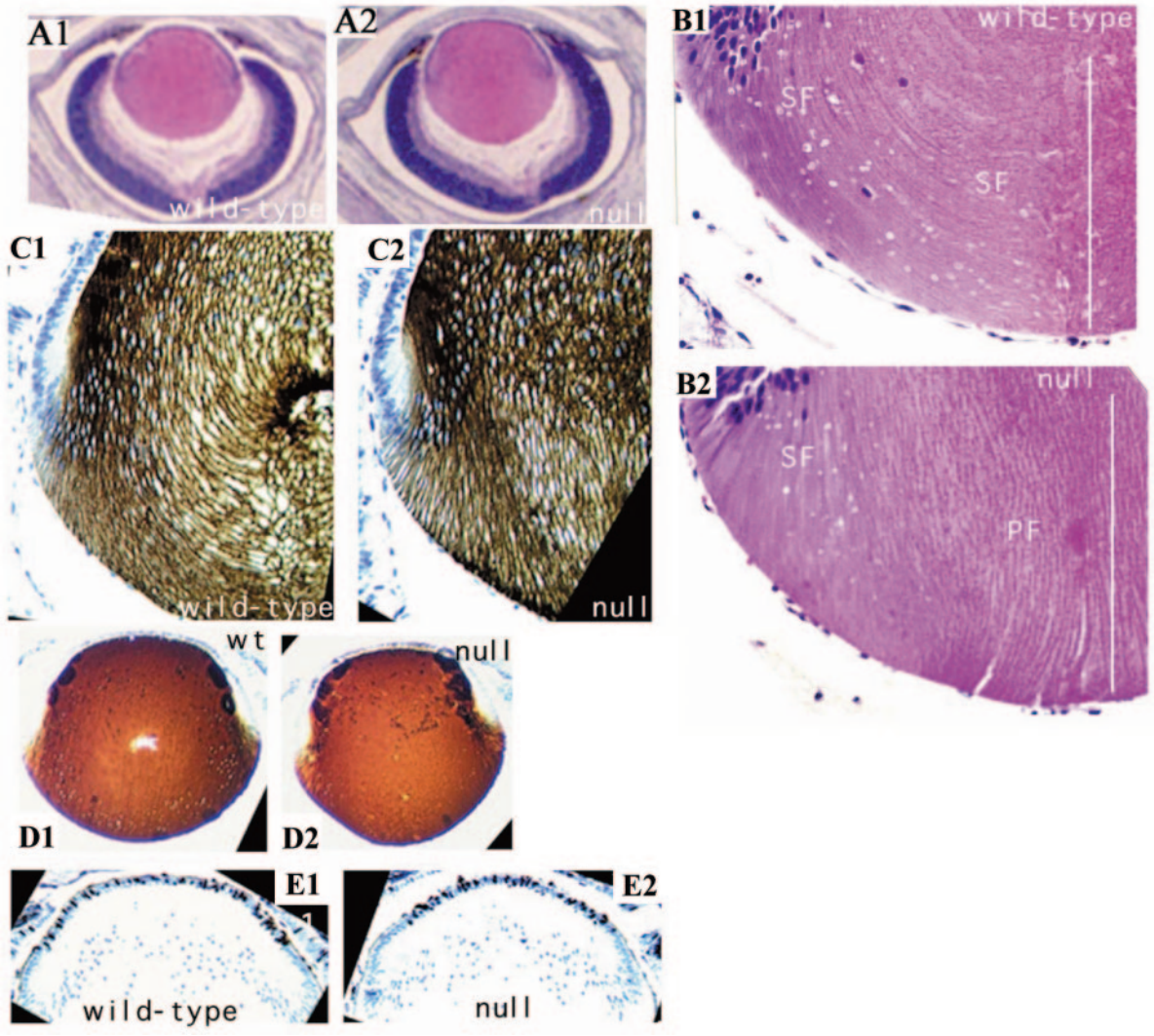

FIG. 2. Defective orientation and migration of secondary lens fibers in E16.5 Abi2 null lens. E16.5 eye sections (5 μm) were cut in the same plane as the optic nerve. In each panel's pair, magnification of wild-type (A1 to E1) and Abi2 null (A2 to E2) sections was the same, and the anterior of the eye in each section is at the top. (A) Whole eye. (B) Lens posterior regions (high magnification of sections in panel A): panel 1, the posterior suture of wild-type secondary lens fibers is to the left of the white line; panel 2, absent posterior suture in Abi2 null lens, to the left of the white line. SF, secondary lens fibers; PF, primary lens fibers. (C to E) Wild-type (C1 to E1) and Abi2 null (C2 to E2) lens sections were processed for immunohistochemistry and stained with anti-MIP26 (C), anti-γ crystallin (D), and anti-BrdU (E).

published data) and/or posttranslational modifications of Abi2 (8). The Abi1 protein was detected as two more-rapidly migrating bands that were unaltered in mobility or concentration levels in the absence of Abi2 (Fig. 1D, lanes 4 to 6, and C, lanes 9 to 12). These data showed the presence of high levels of Abi2 protein in the brain compared to fibroblasts, lack of Abi2 protein expression in the null mice, and normal levels of Abi1 protein in cells or tissues lacking Abi2.

Defective lens development in Abi2 null mice. The eyes of adult Abi2 null mice were markedly smaller than those of wild-type mice, a phenotype that was bilateral and 100% penetrant in inbred C57BL/6 mice, and were consistent in all generations examined. We analyzed whether this phenotype was due to defective lens development. The lens is comprised of two major cell populations: a monolayer of undifferentiated epithelial cells and elongated fiber cells that form the bulk of the lens. By E11.5, a sphere of epithelial cells forms the lens vesicle (44). The epithelial cells in the posterior region exit the cell cycle and differentiate into primary lens fibers, a process that involves extensive cell elongation, enhanced cell-cell interactions, and eventual loss of the nucleus and other membrane-bound organelles (44). Once elongation is complete, the primary lens fibers attach at their posterior to the basement membrane (the lens capsule) and make contact at the anterior with the monolayer of undifferentiated epithelial cells. From E14.5 onwards, anterior epithelial cells withdraw from the cell cycle at the lens equator and each cell, now termed a secondary lens fiber, extends at both the anterior and posterior zones of the lens and around the template provided by the primary fibers (44). At E14.5, in both the wild-type and Abi2 null eyes, the primary lens fibers completely filled the lens vesicle (unpublished data). The wild-type and Abi2 null eyes were of similar size at E16.5 and P1 (Fig. 2A and 3A). However, the orientation and migration of secondary lens fibers in the Abi2

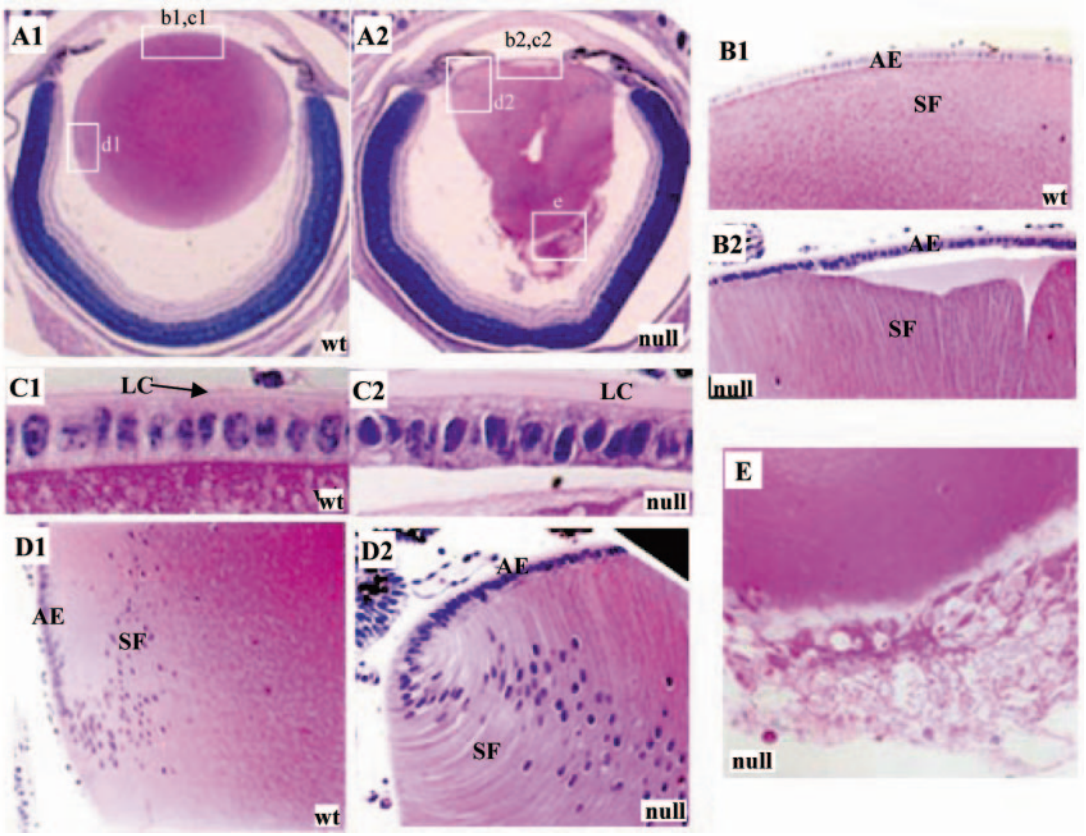

FIG. 3. Abnormal lens phenotypes of postnatal Abi2 null mice. P1 sections of the eye were cut in the same plane as the optic nerve. In each pair, the magnification of wild-type (1) and Abi2 null (2) sections is the same, and the anterior region of each section is at the top. (A) Whole eye of wild-type (A1) and Abi2 null (A2) mice. (B1 and B2) Lens anterior and central region sections are higher magnifications of boxes b1 and b2 in panels A1 and A2, respectively. Note the presence of a V-shaped gap rather than a suture in the null lens (B2). (C1 and C2) Lens anterior and central region sections are higher magnifications of boxes c1 and c2 in panels A1 and A2, respectively. (D1 and D2) Lens equatorial region shown in a higher magnification of boxes d1 and d2 in panels A1 and A2, respectively. (E) Posterior of Abi2 null lens. Shown is a high magnification of boxed region e in panel A2, showing abnormally shaped primary lens fibers released from the broken posterior zone of the Abi2 null lens. AE, anterior epithelial cell layer; SF, secondary lens fibers; LC, lens capsule.

null mice were defective at all of these stages (Fig. 2B and C and 3D). In contrast to wild-type secondary lens fibers, which reoriented and made a 90° turn as they began to migrate, the Abi2 null secondary fibers did not reorient properly (Fig. 2B and C). As a result, in contrast to the concave orientation of the wild-type secondary lens fibers, the secondary fibers in the equatorial region of the Abi2 null lens were oriented in a convex manner (Fig. 2B and C and 3D).

In wild-type lenses, the secondary fibers attach at their anterior tips to the epithelial cell layer and at their posterior tips to the lens capsule. The tips of the fibers migrate towards the poles of the lens, where they detach and form a junction, the lens suture, with the tips of the contralateral migrating secondary fibers (2) (Fig. 2B1 and C1 and Fig. 3B1). In contrast to wild-type lenses, the anterior and posterior sutures failed to form in the absence of Abi2 (Fig. 2B2 and C2 and Fig. 3A2, B2, and E). At P1, the lens was grossly distorted (Fig. 3A) and the lens capsule was markedly thicker in the absence of Abi2 (Fig. 3C). Due to the absence of a suture, the posterior region of the Abi2 null lens was broken open, releasing primary lens fibers and producing gross distortion of the lens (Fig. 3E). Notably, lenses from Abi2 heterozygote mice were indistinguishable from those of wild-type mice (data not shown). Analysis of adult Abi2 null mice revealed the presence of small, round lenses that appeared to have reformed over time.

Defective lens development has been reported to occur as a consequence of aberrant expression of crystallin proteins or as a result of defects in proliferation, differentiation, or apoptosis (38, 42, 81). We investigated these possibilities for the Abi2 null lens. Two lens-specific differentiation markers, MIP26 and γ-crystallin (34, 39), were correctly upregulated in primary and secondary fibers in the absence of Abi2 (Fig. 2C and D), suggesting that differentiation occurs normally. Additionally, pulse labeling of E16.5 embryos with BrdU demonstrated that incorporation of BrdU in the lens was confined to the anterior epithelial cells, as expected (34, 39), and was the same in wild-type and Abi2 null lenses (Fig. 2E), thereby showing that proliferation in the Abi2 null lens is normal. Similar levels of apoptotic cells were detected in the retinas of Abi2 null and wild-type mice (data not shown). As reported (81), the lens did not exhibit appreciable apoptosis, regardless of genotype (data not shown). Thus, the Abi2 null lens phenotype cannot be attributed to aberrant differentiation, proliferation, or apoptosis of lens cells; rather, the data suggest it may be due to

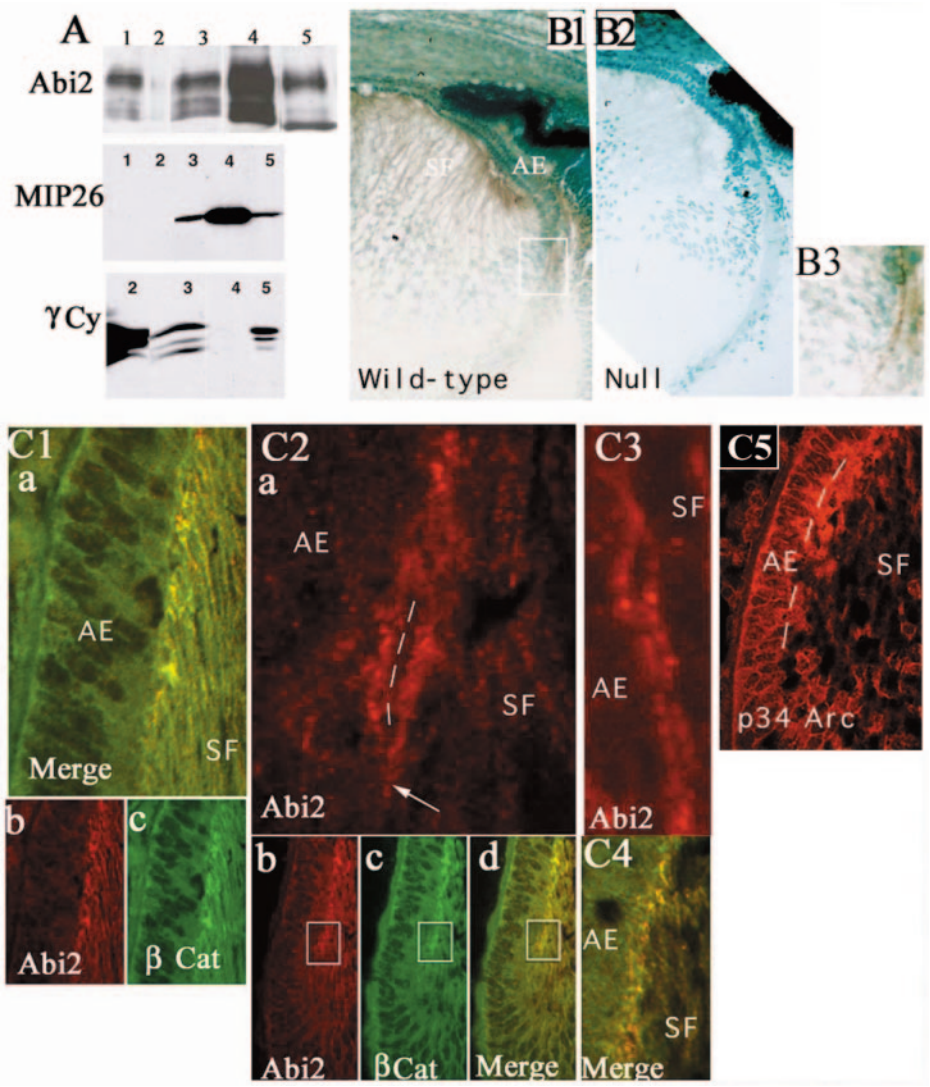

FIG. 4. Localization of Abi2 in the lens during mouse development. (A) Pure lenses from P1 wild-type mice were fractionated. Fractions were separated by SDS-PAGE and blotted with anti-Abi2, anti-MIP26, or anti-γ crystallin (γCy) antibody, as indicated. Lane 1, 100 μg of hypotonic lysate; lane 2, 10 μg of hypotonic lysate; lane 3, 10 μg of CSK lysate; lane 4, 10 μg of RIPA lysate; lane 5, 1/20 of total RIPA-insoluble protein. (B) Wild-type (B1 and B3) and Abi2 null (B2) E18.5 lens sections were processed for immunohistochemistry and stained with anti-Abi2 antibody. Panel B3 shows a high magnification of the boxed region in panel B1. (C) Wild-type E16.5 lens sections were processed for indirect immunofluorescence by using the indicated antibodies, and *Z*-sections were examined by confocal microscopy. In panels C2a and C5, the dotted line delineates the EFI. (C1a) High-magnification merged image of anti-Abi2 (C1b) and anti-β-catenin (C1c) staining. (C2) The boxed regions in panels b, c, and d encompass the transition zone at the beginning of the EFI; panel a shows a higher magnification of the boxed regions in panels b, c, and d. The arrow denotes the beginning of the EFI. (C3 and C4) High magnification of the EFI stained with anti-Abi2 (C3) and costained with antibodies to Abi2 and β-catenin (C4). (C5) High magnification of *Z*-section of the EFI and anterior epithelial cell layer stained with antibodies to the p34 Arc component of the Arp2/3 complex. The dotted line delineates the EFI (C5). AE, anterior epithelial cell layer of the lens; SF, secondary lens fibers.

defective cell adhesion and/or migration. It is also possible that the thickening of the lens capsule in the Abi2 null lens may contribute to the abnormal packing of secondary lens fiber cells and to the rupture of the posterior region observed at P1.

Localization of Abi2 to adherens junctions in the lens and cultured epithelial cells. To gain a better understanding of the secondary lens fiber migration defects observed in Abi2 null mice, we examined the expression and localization of Abi2 in the eye. Abi2 is highly expressed in the eye, particularly in the lens (Fig. 4). In contrast, Abi1 protein was not detected in the lens (data not shown). The localization of Abi2 in wild-type P1 lenses was analyzed by cell fractionation and compared with that of a membrane protein (MIP26) and a cytosolic protein (γ-crystallin) (39). Abi2 was largely insoluble in hypotonic buffer or a buffer used to extract noncytoskeletal proteins but was soluble in RIPA buffer, which releases proteins associated with the membrane-cytoskeletal fraction, such as MIP26 (Fig. 4A). Immunostaining of wild-type lenses with anti-Abi2 antibody showed high levels of Abi2 at the tips of migrating secondary fibers, particularly at the transition zone, where newly differentiating fibers begin their migration along the epithelial cell-fiber interface (EFI) (Fig. 4B1). Control preimmune sera

did not stain wild-type or Abi2 null lenses (data not shown), and the Abi2 null lens did not stain with anti-Abi2 antibody (Fig. 4B2). Abi2 was prominently observed at the cell-cell borders of secondary lens fibers in the anterior of the lens (Fig. 4B1 and C1) and at the base of newly differentiating secondary lens fibers and anterior epithelial cells (Fig. 4B3).

The tips of secondary lens fibers form adherens junctions with anterior epithelial cells at the EFI (32), and mammalian lens fiber cells express a number of junctional proteins, including cadherins and β- and α-catenin (64). Abi2 colocalized with or was adjacent to the adherens junction protein ß-catenin, along secondary lens fiber cell-cell borders (Fig. 4C1 and C2), and at the tips of secondary lens fibers at the EFI (Fig. 4C1 and C4). Abi2 was detected in a double row of puncta at the interface of secondary lens fibers and anterior epithelial cells at the EFI (Fig. 4C2 and C3). The tips of secondary fibers migrate rapidly at the EFI (2), suggesting that dynamic regulation of adherens junctions must occur at this site. Dynamic regulation of adherens junctions involves de novo actin polymerization (69). Thus, we examined the localization of the Arp2/3 actin nucleator complex in the lens. The p34 Arc component of the Arp2/3 complex localized to the EFI in the lens (Fig. 4C5), which is consistent with dynamic regulation of the actin cytoskeleton at this site. Hence, Abi2 localizes to adherens junctions at the EFI, where proteins involved in actin nucleation also accumulate.

To more precisely define the localization of Abi2 during cell-cell junction formation in epithelial cells, we examined these processes in MDCK epithelial cells in vitro. Similar to our findings with fluorescently tagged Abi proteins in melanoma cells and fibroblasts (12, 63), endogenous Abi2 specifically localized at the tips of protruding lamellae in MDCK cells migrating on collagen (Fig. 5A1 to A3). Significantly, Abi2 accumulated at cell-cell contacts, where it colocalized with adherens junction markers β-catenin (Fig. 5B1 to B3), F-actin (Fig. 5C1 to C3), and E-cadherin (data not shown). Abi2 was present at nascent cell-cell junctions, where it clustered adjacent to the tips of F-actin protrusions (Fig. 5D1 to D4). Later during cell-cell junction formation, Abi2 colocalized with adherens junctions markers in puncta (Fig. 5B1 to B3 and C1 to C3), a pattern that is characteristic of developing cell-cell junctions (69). To examine the dynamics of Abi2 localization during cell-cell adhesion, we analyzed the localization of a functional GFP-Abi2B fusion (63) by time-lapse imaging of live MDCK cells. We observed that the levels of GFP-Abi2B at more mature cell-cell junctions (>1 h) were markedly reduced compared to those at earlier junctions (19 to 33 min) (Fig. 5E). This increase in fluorescence intensity was not observed in cells expressing GFP alone (data not shown). These data suggest that, similar to Rac (14), Abi2 may have a role early in adherens junction formation.

Abi proteins modulate adherens junction formation in vitro. To determine whether Abi proteins play a role in the formation of intercellular adhesions in cultured epithelial cells, Abi1 and Abi2 protein expression was downregulated by use of RNA interference in HeLa cells, as both proteins are expressed in these cells. Abi1 and Abi2 were markedly downregulated in HeLa epithelial cells transfected with siRNAs specific for Abi1 and Abi2 (Fig. 6A). Scrambled siRNA controls did not affect Abi protein expression (Fig. 6A) or localization to adherens junctions (Fig. 6B). Abi2 protein failed to accumulate at adherens junctions in cells transfected with Abi siRNAs (Fig. 6B). Significantly, downregulation of Abi1 and Abi2 expression impaired the formation of adherens junctions as assessed by immunostaining with a β-catenin-specific antibody (Fig. 6B). While cells transfected with scrambled siRNA controls displayed a strong and continuous pattern of β-catenin staining at sites of cell-cell adhesion at 2 days posttransfection, loss of Abi protein at these sites in the Abi1/Abi2 siRNA-treated cells resulted in the appearance of finger-like extensions between the adjacent cells, which is characteristic of immature cell-cell junctions (Fig. 6B). Over time, continuous β-catenin was also observed in the cells with downregulated Abi protein expression, supporting a role for Abi proteins during early adherens junction formation (data not shown). The effects on early adherens junction formation observed in cells transfected with the Abi-specific siRNAs were not due to decreased expression of α-catenin or β-catenin, but rather correlated with a marked downregulation of WAVE (Fig. 6C), in agreement with previous findings on the positive role of Abi proteins in the regulation of WAVE protein stability (12, 26, 31, 50). Thus, these data reveal a transient requirement for Abi proteins during formation of nascent adherens junctions in vitro.

Neuroanatomical abnormalities in Abi2 null mice. The Abi2 protein was highly expressed in the brain (Fig. 1) and localized throughout the developing cortex (Fig. 7). Abi2 was prominently expressed in the marginal zone (Fig. 7B), an area rich in neuronal and glial cell processes, and along the border of the lateral ventricles (Fig. 7A1). Interestingly, Abi2 colocalized with β-catenin at cell-cell borders and along the lateral ventricle (Fig. 7A1 to A3). Consistent with the neuronal Abi2 expression, neuroanatomical abnormalities were apparent in both embryonic and adult mice in the absence of Abi2. Aberrant localization of cortical cells into the corpus callosum was observed in Abi2 homozygous null mice at E18.5 (Fig. 8A1 and A2), suggestive of defects in cell migration. Abnormalities in the organization of the neocortex were evident in adult Abi2 null mice, although the normal patterning of the six cortical layers occurred. Invaginations of layer I of the motor cortex were found in Abi2 null mice, and localized heterotopic collections of disorganized neurons were often observed adjacent to the invaginations (4 of 10 mice) (Fig. 8B2 to B4). Pyramidal cells adjacent to the invaginations were not radially oriented as in wild type, but rather were oriented towards the site of invagination (Fig. 8B3 and B4). Also, deeper layers of the motor and visual cortexes exhibited regions of low cellularity that were surrounded by misoriented neurons (Fig. 8C1 and C2). In addition, invaginations of layer I of the cingulate cortex (7 of 10 mice) (Fig. 8D) and visual cortex (1 of 10 mice) (data not shown) were detected in Abi2 null mice. Aberrant localization of cortical cells in layer I of the cingulate cortex was also observed (Fig. 8D). Together, these data are consistent with a role for Abi2 in cell migration and process outgrowth in the developing brain.

The hippocampus of adult Abi2 null mice exhibited mild distortions in organization. In the hippocampus and dentate gyrus, the majority of cells were organized in a laminar architecture resembling that in wild-type mice (Fig. 8F1 and F2). However, in approximately half of the Abi2 null mice, the hippocampal pyramidal layer was periodically interrupted by

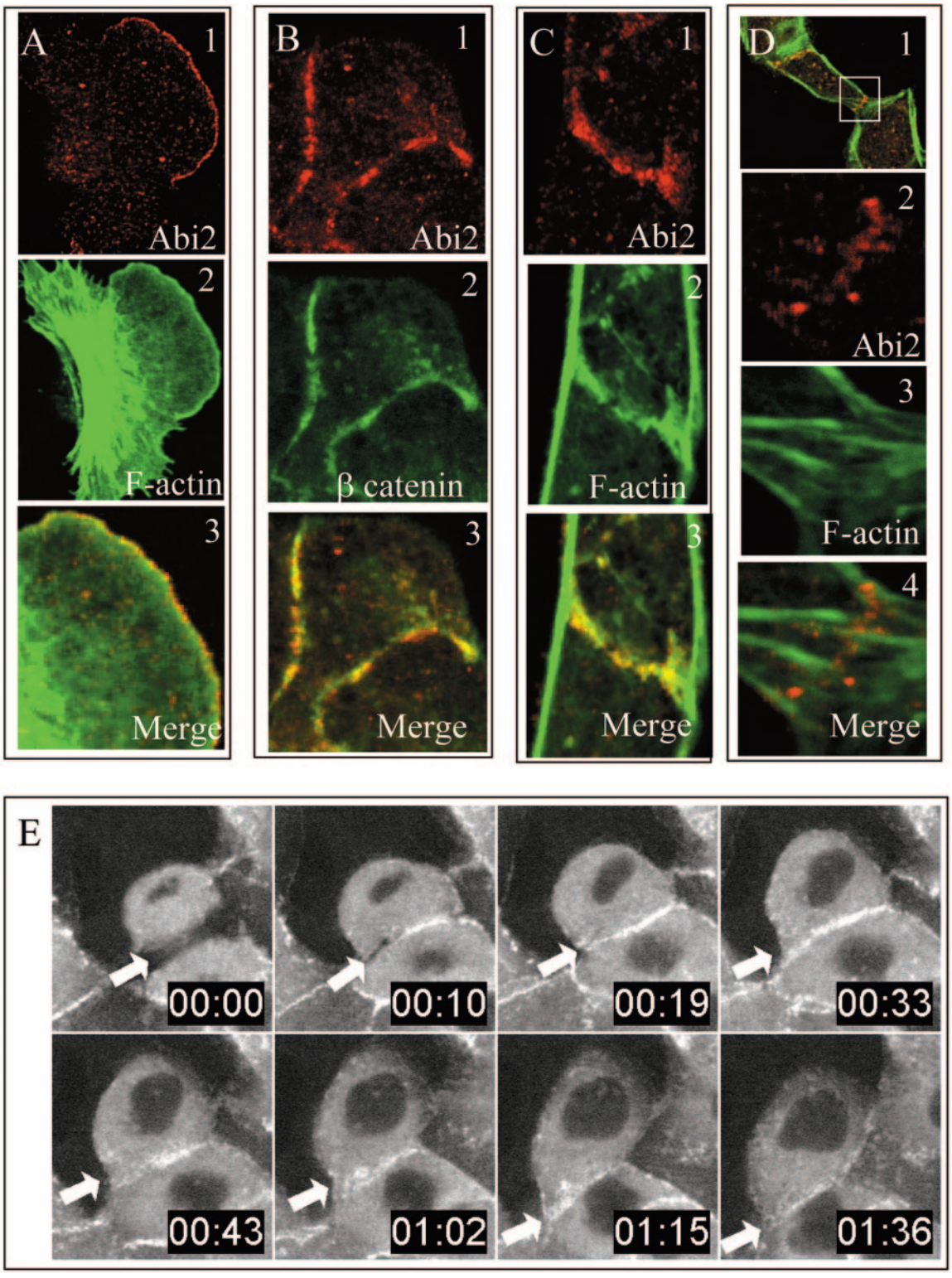

FIG. 5. Localization of Abi2 to nascent adherens junctions in MDCK epithelial cells. MDCK cells in suspension in high-calcium medium were plated onto collagen IV-coated glass coverslips and allowed to migrate and form cell-cell junctions for 1 to 6 h. Cells were processed for indirect immunofluorescence by using the indicated antibodies or phalloidin to stain F-actin. (A) Migrating cell; panel A3 shows a merged image at high magnification of the lamellipodium stained for Abi2 (A1) and F-actin (A2). (B) Colocalization of Abi2 and β-catenin at cell-cell junctions. (C) Colocalization of Abi2 with F-actin at the cell-cell junction but not at the remainder of the cell periphery. (D) Junction formation between three cells. Panels D2 to D4 show higher magnification images of the cell-cell junction boxed in panel D1, stained for Abi2 and F-actin. (E) Time-lapse confocal microscopy of GFP-Abi2B-expressing MDCK epithelial cells. The arrow indicates the accumulation of GFP-Abi2B at adherens junctions. Time is indicated in the form hour:minute.

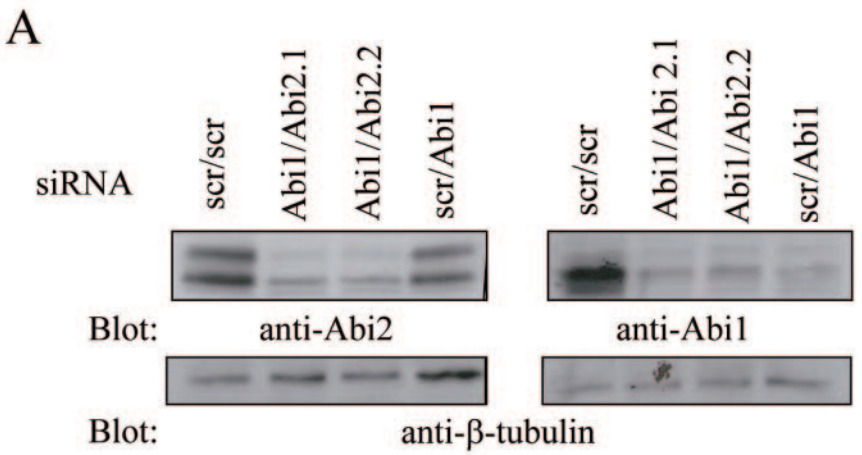
A
siRNA
scr/scr
Abi1/Abi2.1
Abi1/Abi2.2
scr/Abi1
scr/scr
Abi1/Abi 2.1
Abi1/Abi2.2
scr/Abi1
Blot:
anti-Abi2
anti-Abi1
Blot:
anti-β-tubulin

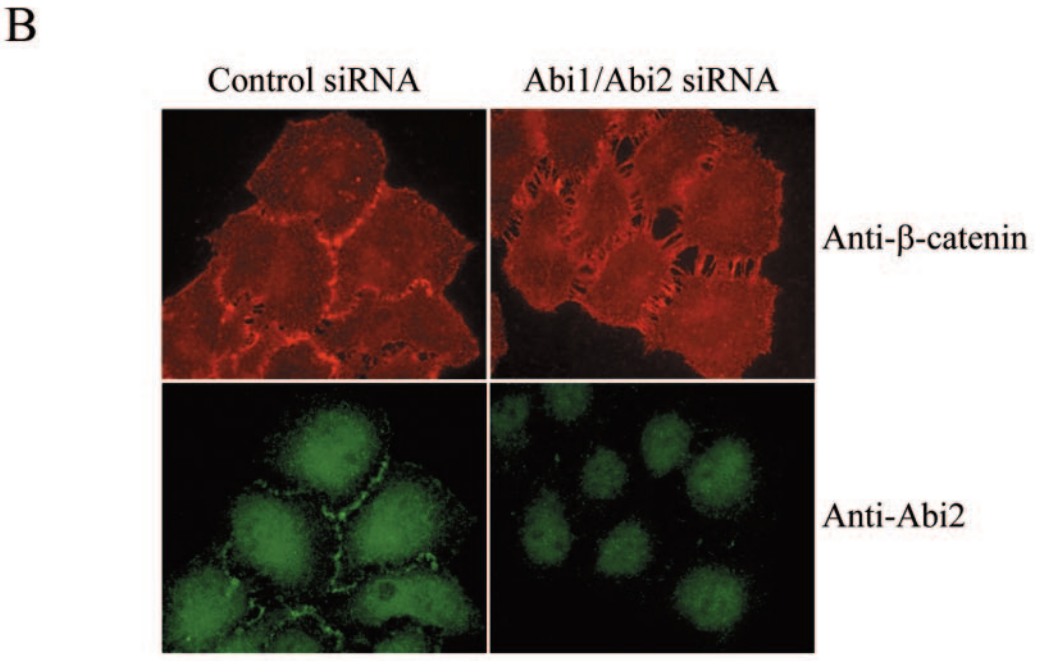
B
Control siRNA
Abi1/Abi2 siRNA
Anti-β-catenin
Anti-Abi2

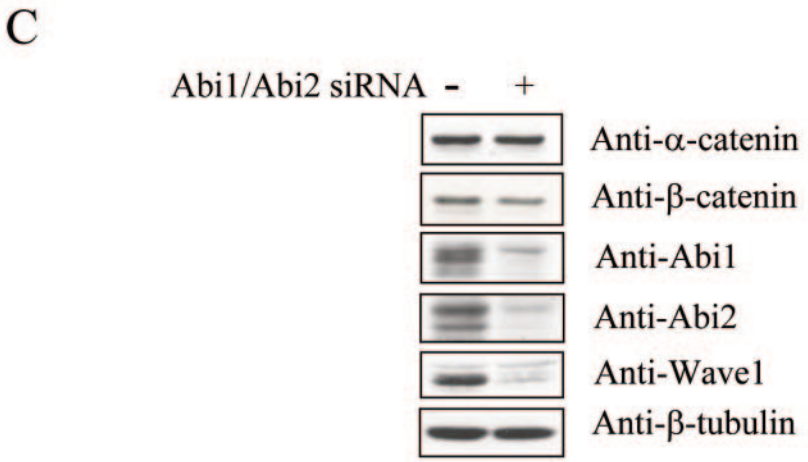
C
Abi1/Abi2 siRNA - +
Anti-α-catenin
Anti-β-catenin
Anti-Abi1
Anti-Abi2
Anti-Wave1
Anti-β-tubulin

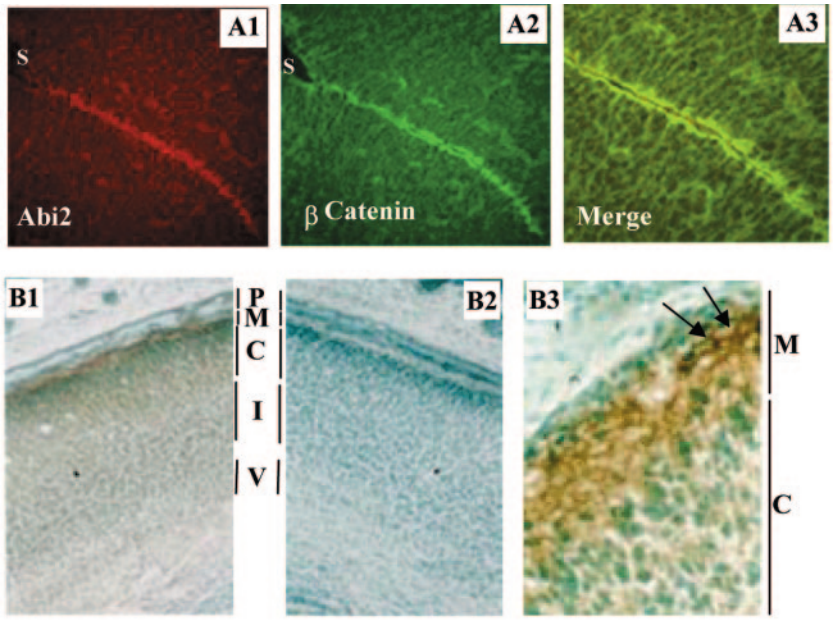

FIG. 7. Localization of Abi2 in the developing mouse brain. (A and B) Coronal cryostat sections (20 μm thick) obtained from embryonic heads were processed for immunofluorescence (A) or immunohistochemistry (B) and incubated with the indicated antibodies (A1 to A3) or anti-Abi2 (B1 to B3). (A) E16.5 frontal cortical section. Shown is the region surrounding the anterior horn of the right lateral ventricle. S, superior part of ventricle. (B) E18.5 frontal cortical sections from wild-type (B1 and B3) and Abi2 null (B2) embryos stained for Abi2 (brown). (B3) High magnification of the marginal zone and cortical plate from panel B1, showing the presence of Abi2 in the cell body and horizontal process of Cajal Retzius-like cells (indicated by arrows) in the marginal zone. P, pia; M, marginal zone; C, cortical plate; I, intermediate zone; V, ventricular zone.

gaps (Fig. 8F2, enlargement of section 1), and granule cells of the dentate gyrus appeared less densely packed and were displaced at discrete sites (Fig. 8F2, enlargement of section 2, and F3), suggestive of cell migration defects.

Defective dendritic spine morphology and density in the absence of Abi2. Abi2 localized to axons and dendrites of wild-type (Fig. 9A1 and B) but not Abi2 null (Fig. 9A2) neurons. Abi2 colocalized with the synaptic markers synaptophysin and synapsin in cortical neurons from E17.5 embryos (data not shown). To determine whether Abi2 was present in dendritic spines, we employed cultured hippocampal neurons from early postnatal wild-type and Abi2 null mice and examined Abi2 localization at different stages of spine development (24, 33). Abi2 staining was strong in dendritic spines of both 14-day in vitro (DIV) (Fig. 9A1 and B1) and 21 DIV (Fig. 9B2) neurons, but it was weak in filopodia, which are precursors to dendritic spines (data not shown). In some cases, Abi2 staining was intense in the central portion of the spine (Fig. 9A1 and B1), whereas in other spines, Abi2 immunofluorescence staining appeared as doublets that sometimes were directly apposed by axonal Abi2 staining (Fig. 9B).

Given the localization of Abi2 to dendritic spines in vitro, we examined the morphology and density of dendritic spines in wild-type and Abi2 null mice in vivo. Adult mice brains were impregnated according to the Golgi procedure (55), and fully impregnated neurons were analyzed. Basal dendrites of pyramidal neurons in layers III and V of the somatosensory cortex and the CA1 region of the hippocampus were examined. On basal dendrites of layer III pyramidal neurons in Abi2-deficient mice, there was a significant decrease ($P < 0.05$, Student's t test, one tailed) in the relative proportion of spines that were of mushroom-type morphology (56% wild-type, 42% Abi2 null, and 39% Abi2 heterozygous) and a corresponding increase in the proportion of stubby spines (25% wild type, 36% Abi2 null, and 38% Abi2 heterozygous) (Fig. 9C). However, the density of spines on basal dendrites was similar in wild-type (74 spines/100 μm) and Abi2 null (76 spines/100 μm) mice. Notably, the density of spines on apical dendritic branches of layer V pyramidal cells was significantly lower in Abi2 null mice (76 spines/100 μm) and Abi2 heterozygous mice (44 spines/100 μm) compared to wild-type mice (100 spines/100 μm). Spine density of apical dendritic branches in the CA1 region of the hippocampus was also significantly decreased in Abi2 null mice (45 spines/100 μm) and in Abi2 heterozygous mice (42 spines/100 μm) compared to wild-type mice (85 spines/100 μm) (Fig. 9D and E).

FIG. 6. Downregulation of Abi expression impairs adherens junction formation in epithelial cells. (A) HeLa cells were transfected with a 100 nM concentration of the indicated siRNAs specific for Abi1 and/or Abi2 (Abi2.1 and -2.2), or with scrambled control siRNA. After 48 h, the cells were lysed and Abi protein levels were determined by Western blotting with the indicated anti-Abi antibodies. The blots were stripped and reprobed with β-tubulin antibody to show equal protein loading. (B) HeLa cells were cotransfected with 100 nM siRNA mix containing siRNAs for Abi1 and Abi2 or scrambled siRNA control (200 nM) as indicated. After 48 h, the cells were approximately 75% confluent and were fixed, permeabilized, and stained for β-catenin or for Abi2 as indicated. The results shown are representative of five independent experiments, with each transfection done in duplicate or triplicate. (C) HeLa cells transfected with scrambled or Abi1/Abi2 siRNAs were lysed at 48 h posttransfection, and the lysates were blotted for the indicated antibodies.

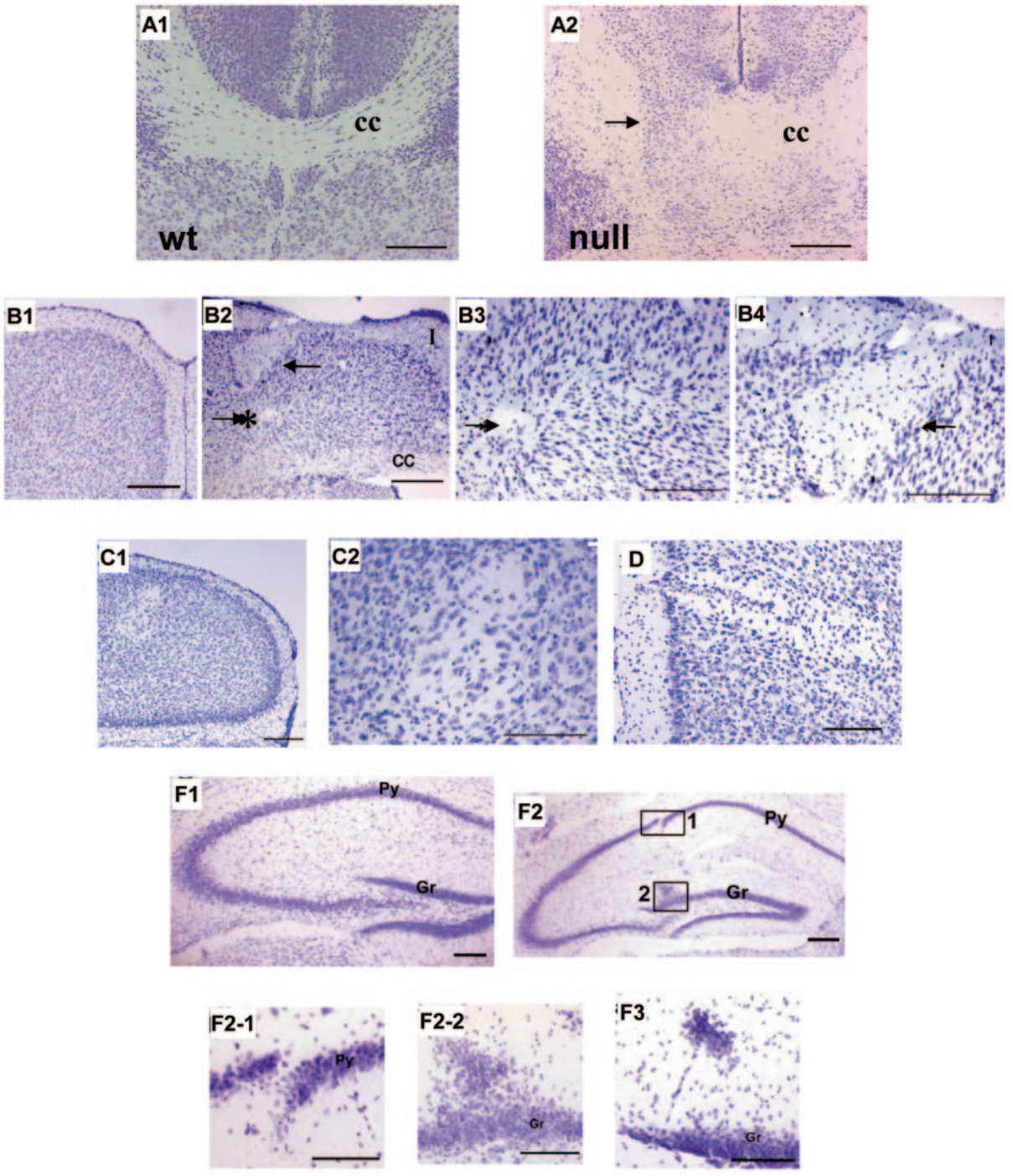

FIG. 8. Morphological defects in the neocortex and hippocampus of Abi2 null mice. (A) Nissl-stained coronal sections (20 μm) of wild-type (A1) and Abi2 null (A2) neocortexes at E18.5 in the region of the corpus callosum (cc). In the wild-type mice (A1), the cells of the cortical plate form a distinct line above the corpus callosum, whereas these cells are displaced into the corpus callosum in Abi2 null mice (arrow). (B to F) Nissl-stained coronal sections (40 μm) of wild-type (B1 and F1) and Abi2 null (B2 to B4, C, D, F2 and F3) adult mouse brain from corresponding anatomical levels. (B) Comparison of wild-type (B1) and Abi2 null (B2-4) motor cortexes. Panels B3 and B4 are higher magnification images of B2. (B2 and B3) Invaginations of layer I (upper arrow). (B2 and B4) Misplacement of layer I within deeper layers of the cortex adjacent to the invagination (lower arrow). Note the aberrant, almost horizontal orientation of neurons towards the misplaced layer I. In panel B4, compare the cell orientation in the lower half to the right of the arrow with the orientation in the upper half. Py, pyramidal cell layer; Gr, granule cell layer; I, layer I of the neocortex; CC, corpus callosum. (C) Aberrant cellular orientation around cell-poor regions in the visual cortex of Abi2 null mice. Panel C2 is a higher magnification of the image in panel C1. (D) Invagination of layer I in the cingulate cortex of Abi2 null mice, with layer I to the left. (F) Comparison of wild-type (F1) and Abi2 null (F2 and F3) hippocampus sections. (F2-1 and F2-2) are higher magnifications of boxed regions 1 and 2, respetively, in panel F2. (F3) Higher-magnification image of the dentate gyrus of a different Abi2 null mouse. Bars = 100 μm.

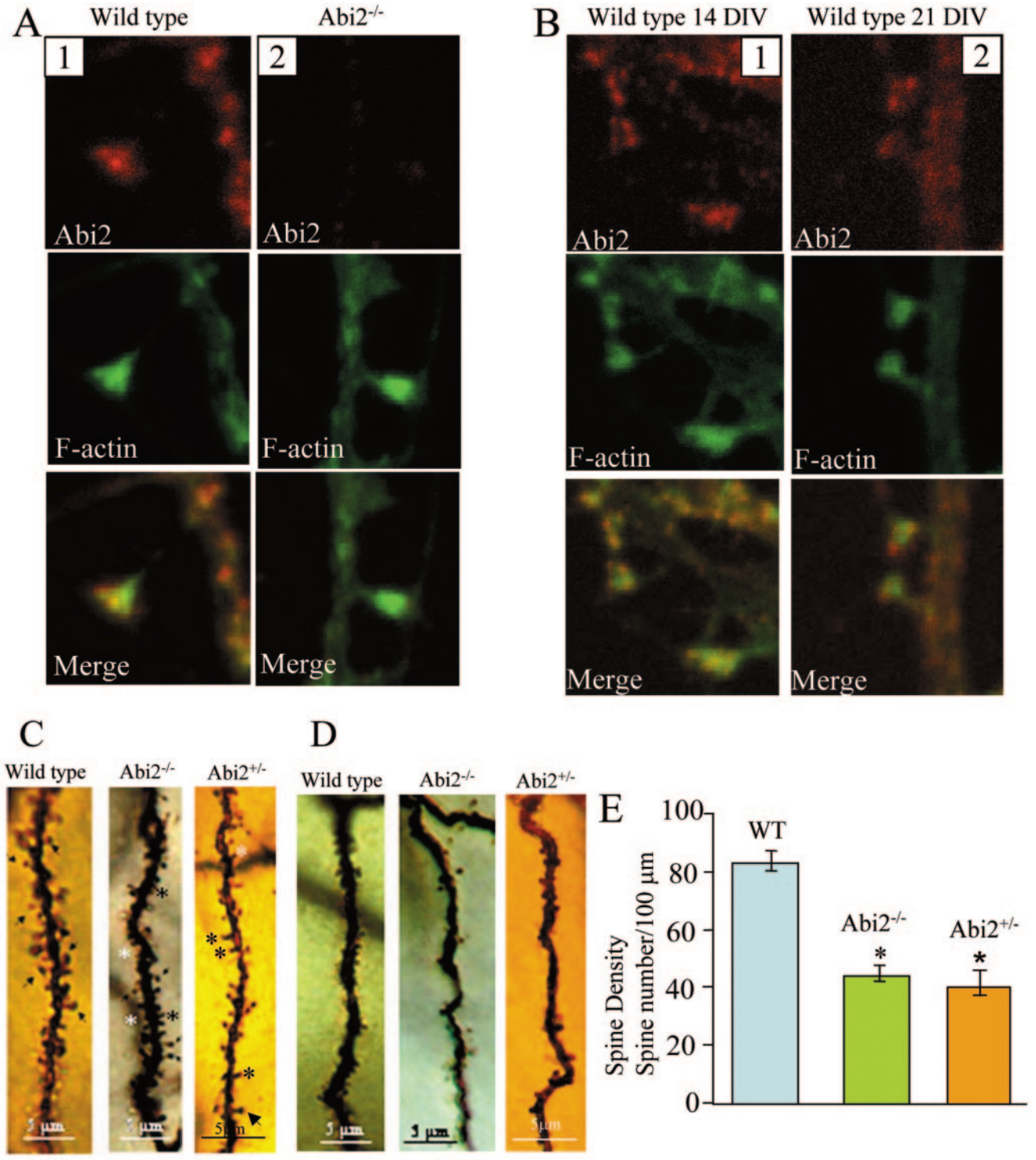

FIG. 9. Loss of Abi2 results in aberrant spine morphology and density. (A and B) Primary neurons from P2 hippocampus were isolated from wild-type or Abi2$^{-/-}$ mice and cultured in vitro for either 14 (A and B1) or 21 (B2) days. Localization of Abi2 (red) at dendritic spines is visualized by intense costaining with F-actin (green). (A) Abi2 staining of dendritic spines from 14-DIV wild-type neurons (A1) but not Abi2 null hippocampal neurons (A2). Panels for wild-type and Abi2 null neurons were taken using identical confocal magnification and intensity settings. Note the intense dot of Abi2 staining at the center-front of the wild-type spine. (B) Abi2 staining of dendritic spines in wild-type hippocampal neurons grown for 14 DIV (B1) or 21 DIV (B2). (C to E) Analysis of dendritic spines in pyramidal neurons of adult wild-type, Abi2$^{-/-}$, and Abi2$^{+/-}$ neocortexes and CA1 regions of the hippocampus by the Golgi impregnation procedure. Three to five mice of each genotype were employed for the analyses. (C) Representative images of basal dendrite branches of wild-type, Abi2$^{-/-}$, and Abi2$^{+/-}$ pyramidal neurons of layer III of the somatosensory cortex. Arrows denote mushroom spines, and asterisks denotes stubby spines. (D) Representative images showing density of dendritic spines on side branches of apical dendrites for wild-type, Abi2$^{-/-}$, and Abi2$^{+/-}$ CA1 hippocampal pyramidal neurons. (E) Quantification of spine density from panel D expressed as the mean number of spines per 100 μm of dendritic length.

Impaired learning and memory in Abi2-deficient mice. The synaptic localization of Abi2, in particular its localization to dendritic spines, and the dendritic spine defects in the Abi2 null mice suggested that memory formation may be impaired in the absence of Abi2. To address this possibility, behavioral tests were performed with wild-type, Abi2$^{+/-}$ and Abi2$^{-/-}$ mice. Deficits in short- and long-term memory have been characterized with a one-trial passive avoidance test (70). In this assay, foot shock is used to train mice to refrain from crossing from a lighted to a darkened chamber. Latency to cross to the darkened chamber after conditioning is used as an index of memory consolidation and retention. Initial neurophysiological tests of Abi2$^{-/-}$ mice showed that rudimentary sensory and motor functions were within the normal range of mouse behaviors. Abi2$^{-/-}$ mice have eyes that are smaller than wild-type mice. To determine whether rudimentary visual responses were intact in Abi2-deficient mice, animals were evaluated for pupillary responses, their ability to track a moving object, and light-dark discrimination. In all three tests, no differences were discerned for wild-type, Abi2$^{-/-}$, and Abi2$^{+/-}$ mice; all animals displayed pupillary responses to light, could track a moving object, and could discriminate light from dark (data not shown). In the latter test, all animals rapidly entered a darkened chamber and stayed in this chamber for approximately 2 min. Thereafter, the numbers of transitions between the light and dark chambers and the time spent in each chamber were virtually identical for the three genotypes (data not shown). Hence, adult Abi2 null and heterozygous mice did not have detectable impairment of gross visual functions for orientation, object tracking, visual placement, and dark-light discrimination (data not shown). No differences were discerned in the abilities of the three genotypes of mice to sense and respond to foot shock (Fig. 10A). During passive avoidance training, wild-type, Abi2$^{+/-}$, and Abi2$^{-/-}$ mice were equally likely to cross rapidly to the darkened chamber (Fig. 10B). However, when tested at 0.5, 1, or 24 h later, wild-type mice showed substantially longer latencies to cross to the darkened chamber relative to Abi2$^{+/-}$ and Abi2$^{-/-}$ mice (Fig. 10B). These data show that Abi2$^{+/-}$ and Abi2$^{-/-}$ mice are deficient in short- and long-term memory formation. To investigate whether additional exposure to the task would improve the performance of Abi2-deficient mice, animals that were initially tested at the 1-h retention were retrained and retested 7 days later (final test). During retraining, approximately 86% of each genotype readily crossed to the darkened chamber (Fig. 10C). Retesting showed that although wild-type animals showed the longest latency to cross to the darkened chamber, the latency was not significantly greater than that of Abi2$^{+/-}$ mice (Fig. 10C). Indeed, comparisons between initial and final testing revealed that while retraining did not significantly improve wild-type performance, latencies for Abi2$^{+/-}$ mice were significantly increased (Fig. 10B and C). Although latency scores for Abi2$^{-/-}$ mice were not significantly different at retesting compared to initial testing, there was a trend towards increased latency (Fig. 10B and C).

To examine behaviors of individual mice during the retesting for passive avoidance, their patterns of chamber entry were analyzed over a 300-s test interval. While retesting increased the latencies in crossing to the darkened chamber for Abi2$^{+/-}$ and Abi2$^{-/-}$ mice (Fig. 10C), the individual response patterns revealed that these mice were still deficient on this task (Fig. 10D). While 75% of wild-type mice did not cross to the darkened chamber, only 57% of Abi2$^{+/-}$ and 25% of Abi2$^{-/-}$ mice showed this behavior. The remaining 43% of Abi2$^{+/-}$ mice and 75% of Abi2$^{-/-}$ mice rapidly entered the dark chamber (Fig. 10D). In summary, the passive-avoidance data show that Abi2$^{+/-}$ and Abi2$^{-/-}$ mice are deficient in both short- and long-term memory formation but that retraining can improve performance, particularly in Abi2$^{+/-}$ mice.

DISCUSSION

In this work we uncovered a role for Abi2 in the regulation of cell morphogenesis in vivo. Homozygous deletion of murine *abi2* produces abnormal phenotypes in the eye. Lens morphogenesis is an excellent system for analyzing the interplay of cell adhesion, migration, differentiation, proliferation, and survival (44). Morphogenesis of the lens involves dramatic changes in actin cytoskeleton organization to allow for cell elongation, cell adhesion turnover, and migration. We have shown that the most striking and penetrant phenotype induced by homozygous loss of Abi2 is the incorrect orientation and migration of secondary lens fibers without affecting differentiation, proliferation, or survival in the lens. This phenotype is consistent with the localization of Abi2 at the interface of secondary lens fibers and the undifferentiated epithelial cells. Defective actin polymerization at this site in the absence of Abi2 may underlie the inability of the secondary lens fibers to orient properly and migrate to form a suture with the tips of contralateral secondary fibers, thereby producing a gap at the anterior of the P1 lens. Loss of Abi2 may also result in defective intercellular adhesion, as Abi2 may link cadherin activation during formation of adherens junctions to remodeling of the actin cytoskeleton. A role for cadherin-mediated adhesion in cell migration has been demonstrated for border cell migration during *Drosophila* oogenesis (54) and for muscle cell migration in the developing zebrafish myotome (7). Our findings in vitro and in vivo suggest that defective intercellular adhesion in the absence of Abi2 may contribute to altered cell migration and defective morphogenesis in the murine lens.

Development of cadherin-dependent epithelial cell-cell adhesion is driven by lamellipodia in living cells (14). Here we showed that Abi2 is enriched at adherens junctions and that as adherens junctions mature, Abi2 accumulation diminishes at these sites. This pattern of localization is similar to that of Rac (14). Thus, Abi2 may function in concert with Rac during intercellular junction formation rather than maintenance. A role for Abi proteins in the formation of adherens junctions is further supported by our finding that downregulation of endogenous Abi proteins by RNA interference impairs early adherens junction formation. The effect of Abi downregulation on adherens junction formation in HeLa epithelial cells is transient, which suggests that other proteins that accumulate at these structures may play redundant roles. Indeed, inhibition of adherens junctions in vitro has been reported to occur as a consequence of functional disruption of a subset of signaling molecules implicated in the regulation of the actin cytoskeleton, such as the Vasp/Ena protein family, the Rho GTPases, Dia1, and formin1 (18, 29, 51, 69). These reports underscore the importance of adhesion-mediated changes in the actin cy-

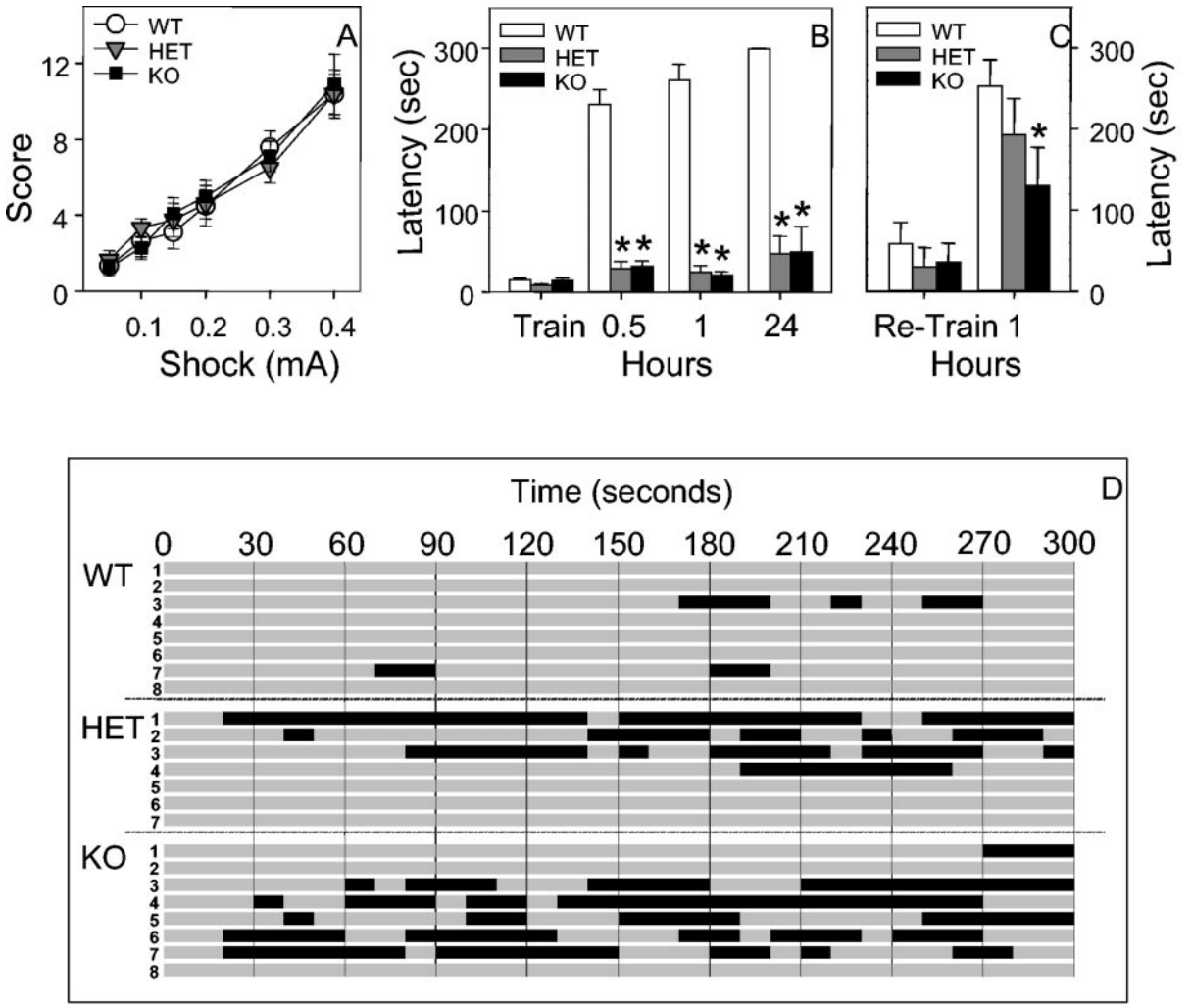

FIG. 10. Defective memory formation in Abi2-deficient mice. (A) Sensitivity of wild-type, Abi2$^{+/-}$, and Abi2$^{-/-}$ mice to scrambled foot shock; each genotype behaved in a similar manner. (B and C) Passive avoidance testing: shown is the latency (in seconds) to enter the darkened chamber from the lighted chamber during training and at 30 or 60 min or 24 h after training; $n = 7$ to 10 mice for each genotype. (B) During initial testing, all naive mice rapidly crossed to the dark chamber. However, at 30 or 60 min or 24 h after training, wild-type mice did not readily cross to the dark chamber, while Abi2$^{+/-}$ and Abi2$^{-/-}$ mice readily crossed. *, $P < 0.05$ versus wild-type controls. (C) Since Abi2$^{+/-}$ and Abi2$^{-/-}$ mice showed poor retention in initial testing, animals that were initially tested for a 1-h retention were retrained and retested at that same (1-h) retention interval 1 week later. Note that there was still a tendency (*, $P < 0.06$) for Abi2$^{-/-}$ mice to enter the dark chamber more readily than wild-type animals. (D) Individual recordings depicting crossing and duration of time spent (maximal time allowed = 300 s) in the lighted (grey bars) and dark (black bars) chambers by wild-type ($n = 8$), Abi2$^{+/-}$ ($n = 7$), and Abi2$^{-/-}$ ($n = 8$) mice during the 1-h retention test following retraining and retesting for passive avoidance.

toskeleton for the formation and integrity of adherens junctions.

How does Abi2 regulate lamellipodia-driven adherens junction formation? Lamellipodial protrusions are dependent on Rac activation (16), and Abi proteins have been linked to signaling complexes upstream and downstream of Rac. Abi proteins may stimulate the activity of specific GEF proteins towards Rac, as reported previously (25, 56, 57). Alternatively, Abi proteins may be involved in targeting Rac-GEFs to specific membrane sites to initiate signaling cascades leading to induction of de novo actin polymerization. Abi family proteins may also affect lamellipodial protrusions by regulating WAVE function downstream of Rac. Similar to Abi, WAVE proteins accumulate at the tips of protruding lamellipodia (22, 65). WAVE stimulates the actin nucleating activity of the Arp2/3 complex in response to Rac activation, and loss of WAVE function impairs lamellipodia formation in *Drosophila* and mouse cells (13, 31, 50, 65). Recently, downregulation of *Drosophila* Abi and mammalian Abi1 in vitro in cells was shown to inhibit formation of lamellipodia, possibly due to increased degradation and/or mislocalization of WAVE (26, 31, 50). Consistent with these findings, we showed that downregulation of Abi protein expression by RNA interference leads to reduced WAVE levels. Interestingly, we have identified naturally occurring forms of Abi2 that lack N-terminal sequences required for WAVE binding and localization to the tips of lamellipodia (unpublished results). This finding suggests that regulated expression of Abi2 proteins encoding or lacking these N-terminal sequences could affect actin polymerization at the leading edge during development or under pathological

conditions. Moreover, abnormal lens morphogenesis and defective cell migration in vivo in mice lacking Abi2 are consistent with the findings that *C. elegans* orthologs of Nap1/Nap125 and PIR121, two protein components of the Rac-responsive WAVE/Abi complex, regulate tissue morphogenesis and cell migration in vivo (61) and that WAVE2 regulates migration, sprouting, and branching of endothelial cells during mouse development (76).

Abnormalities in the reorganization of the actin cytoskeleton may also underlie the neuronal abnormalities present in Abi2-deficient mice. These mice exhibited highly penetrant and profound impairments in short- and long-term memory. These deficits were accompanied by abnormalities in dendritic spine morphology and density in Abi2 null and Abi2 heterozygous mice. Changes in spine morphology and number have been correlated with alterations in behavior and may provide a morphological basis for synaptic plasticity (33, 79). Dendritic spine morphology is developmentally regulated, progressing from filopodial in early development to mushroom-shaped spines with an expanded head connected to the dendrite shaft by a narrow neck in the mature brain (24). Dendritic spines may exhibit additional shapes, such as stubby spines that lack the neck and thin (headless) spines (24). We showed that basal dendrites of layer III pyramidal neurons of Abi2-deficient mice exhibited a significant decrease in the relative proportion of mushroom-shaped spines and a corresponding increase in the proportion of stubby spines. The functional consequences of this morphological change are unclear, but shortening of the spine neck may change synaptic strength (66). Moreover, spine density on apical dendritic branches of layer V pyramidal cells and in the CA1 region of the hippocampus was significantly reduced in Abi2-deficient mice compared to wild-type mice. Abi2 was expressed in both axons and dendritic spines. Therefore, the reduced spine density in the Abi2-deficient mice might be due to loss of presynaptic and/or postsynaptic Abi2 functions.

Abnormalities in dendritic spine morphology and density similar to those presented by the Abi2-deficient mice have been observed in vitro after expression of dominant-negative Rac or dominant-negative PIX, a GEF for Rac (41, 80). Expression of dominant-negative Rac in hippocampal slice cultures produces a decrease in spine density, with some dendrites lacking spines altogether (41). Expression of dominant-negative forms of PIX or the PIX-binding protein GIT1 results in a significant decrease in the number of normal mushroom-shaped spines in cultured hippocampal neurons (80). These findings underscore the critical requirement for Rac signaling in the regulation of dendritic spine morphogenesis and synapse formation. We propose that the absence of Abi2 results in defects in Rac-dependent pathways involved in the regulation of actin dynamics, producing deficits in spine morphology and density.

Alterations in dendritic spine morphology may also result by interfering with the function of cell surface receptors that control intercellular adhesion such as N-cadherin and the Eph receptor tyrosine kinases. Interfering with the function of these receptors results in the replacement of normal mushroom-shaped dendritic spines with long thin spines, filopodia, or immature small-headed or headless spines (15, 23, 40, 68). Our finding that endogenous Abi2 localizes to cadherin-dependent adherens junctions suggests that Abi2 may function downstream of cadherins during synapse formation. This possibility is further supported by recent reports showing that β-catenin and α-N-catenin regulate dendritic spine morphogenesis in vitro (1, 78). Abi1 has also been linked to ephrin-B1, a membrane-bound ligand for the EphB2 receptor tyrosine kinase. Abi1 binds to Grb4/Nckβ, an adaptor protein that interacts with the tyrosine-phosphorylated intracellular tail of ephrin-B1 (9). Ephrins are both pre- and postsynaptic (6, 21), and ephrin-B proteins are highly expressed in postsynaptic CA1 hippocampal neurons and are required for synaptic plasticity (21). It is possible that the absence of Abi2 at sites of interneural adhesion elicits altered synaptic connectivity downstream of several adhesion receptor systems, possibly by blocking the signaling pathways that link the activation of the adhesion receptors to Rac-dependent regulation of actin dynamics at dendritic spines.

It is significant that several genes encoding regulators and effectors of the Rho family GTPases are mutated in patients with syndromic and nonsyndromic forms of mental retardation (46). Among regulators and effectors of Rho GTPases, LIMK1, oligophrenin, and αPIX all have been shown to regulate dendritic spine morphogenesis (20, 35, 80). Furthermore, mice that are homozygous null for WAVE1 exhibit deficits in learning and memory, despite the absence of obvious abnormalities in the cellular organization of the hippocampus (60). These findings suggest functional links between Abi2 and WAVE1 in the regulation of cognitive functions and are consistent with the presence of Abi2 in a protein complex with WAVE1, Nap1, and PIR121/Sra-1 (13, 26, 59, 62). In this regard, the PIR121/Sra-1 proteins bind to the fragile X mental retardation protein FMRP (52), and the fly ortholog of Sra-1 regulates axonal pathfinding and synaptic morphology and interacts biochemically and genetically with the *Drosophila* orthologs of Rac and FMR1 (53). Interestingly, WAVE1 binds to the c-Abl tyrosine kinase (74), and c-Abl binds and phosphorylates Abi2 (10). Thus, it is possible that WAVE1 and Abi2 function in a coordinated manner to integrate Rac- and Abl kinase-dependent signaling pathways at neuronal synapses (37, 41, 46). As dendritic spine plasticity has been linked to memory formation (79), an exciting possibility is that the memory defects in Abi2-deficient mice may be due to the aberrant regulation of pathways that link neuronal connectivity mediated by adhesion receptors to Rac-dependent actin reorganization.

ACKNOWLEDGMENTS

We thank Cheryl Bock at the DUMC Transgenic Mouse Facility for the generation of the Abi2 null mice. We are grateful to Philippe Soriano for advice in the preparation of the targeting construct and the kind gifts of the pPGKneobpAloxPGKDTA vector and the 129 Sv mouse genomic DNA library. We thank Frank Gertler for electroporation of the targeting construct into ES cells and Kevin D. Courtney for advice. We are grateful to Sam Zigler for the anti-MIP26 and anti-γ crystallin antibodies and Matthew Welch for the anti-p34 Arc antibody. We thank Guoping Feng, Michael Ehlers, Anthony-Samuel La Mantia, Vasanth Rao, Joseph Costello, and Gordon Klintworth for insightful suggestions and Anthony Means and Tso-Pang Yao for critical reading of the manuscript.

This work was supported in part by National Institutes of Health grants R01 CA70940 and GM62375 to A.M.P. and R01 HD35170 and NS26620 to P.F.M., by grant 12-FY99-468 from the March of Dimes Birth Defects Foundation, and by a grant from the National Alliance for Research on Schizophrenia and Depression to W.C.W.

REFERENCES

1. **Abe, K., O. Chisaka, F. van Roy, and M. Takeichi.** 2004. Stability of dendritic spines and synaptic contacts is controlled by βN-catenin. Nat. Neurosci. **7:** 357–363.
2. **Bassnett, S., H. Missey, and I. Vucemilo.** 1999. Molecular architecture of the lens fiber cell basal membrane complex. J. Cell Sci. **112:**2155–2165.
3. **Biesova, Z., C. Piccoli, and W. T. Wong.** 1997. Isolation and characterization of e3B1, an eps8 binding protein that regulates cell growth. Oncogene **14:** 233–241.
4. **Blagg, S. L., M. Stewart, C. Sambles, and R. H. Insall.** 2003. PIR121 regulates pseudopod dynamics and SCAR activity in *Dictyostelium.* Curr. Biol. **13:** 1480–1487.
5. **Chelly, J., and J. L. Mandel.** 2001. Monogenic causes of X-linked mental retardation. Nat. Rev. Genetics **2:**669–680.
6. **Contractor, A., C. Rogers, C. Maron, M. Henkemeyer, G. T. Swanson, and S. F. Heinemann.** 2002. *trans*-synaptic Eph receptor-Ephrin signaling in hippocampal mossy fiber LTP. Science **296:**1864–1869.
7. **Cort,s, F., D. Dagget, R. J. Bryson-Richardson, C. Neyt, J. Maule, P. Gautier, G. E. Hollway, D. Keenan, and P. Currie.** 2003. Cadherin-mediated differential cell adhesion controls slow muscle cell migration in the developing zebrafish myotome. Dev. Cell **5:**865–876.
8. **Courtney, K. D., M. Grove, H. Vandongen, A. Vandongen, A. S. LaMantia, and A. M. Pendergast.** 2000. Localization and phosphorylation of Abl-interactor proteins, Abi-1 and Abi-2, in the developing nervous system. Mol. Cell. Neurosci. **16:**244–257.
9. **Cowan, C. A., and M. Henkemeyer.** 2001. The SH2/SH3 adaptor Grb4 transduces B-ephrin reverse signals. Nature **413:**174–179.
10. **Dai, Z., and A. M. Pendergast.** 1995. Abi-2, a novel SH3-containing protein interacts with the c-Abl tyrosine kinase and modulates c-Abl transforming activity. Genes Dev. **9:**2569–2582.
11. **Demyanenko, G. P., A. Y. Tsai, and P. F. Maness.** 1999. Abnormalities in neuronal process extension, hippocampal development, and the ventricular system of L1 knockout mice. J. Neurosci. **19:**4907–4920.
12. **Echarri, A., M. J. Lai, M. R. Robinson, and A. M. Pendergast.** 2004. Abl interactor 1 (Abi-1) Wave-binding and SNARE domains regulate its nucleocytoplasmic shuttling, lamellipodium localization, and Wave-1 levels. Mol. Cell. Biol. **24:**4979–4993.
13. **Eden, S., R. Rohatgi, A. V. Podtelejnikov, M. Mann, and M. W. Kirschner.** 2002. Mechanism of regulation of WAVE1-induced actin nucleation by Rac1 and Nck. Nature **418:**790–793.
14. **Ehrlich, J. S., M. D. Hansen, and W. J. Nelson.** 2002. Spatio-temporal regulation of Rac1 localization and lamellipodia dynamics during epithelial cell-cell adhesion. Dev. Cell **3:**259–270.
15. **Ethell, I. M., F. Irie, M. S. Kalo, J. R. Couchman, E. B. Pasquale, and Y. Yamaguchi.** 2001. EphB/syndecan-2 signaling in dendritic spine morphogenesis. Neuron **31:**1001–1013.
16. **Etienne-Manneville, S., and A. Hall.** 2002. Rho GTPases in cell biology. Nature **420:**629–635.
17. **Fan, P. D., and S. P. Goff.** 2000. Abl interactor 1 binds to Sos and inhibits epidermal growth factor- and v-Abl-induced activation of extracellular signal-regulated kinases. Mol. Cell. Biol. **20:**7591–7601.
18. **Fukata, M., and K. Kaibuchi.** 2001. Rho-family GTPases in cadherin-mediated cell-cell adhesion. Nat. Rev. Mol. Cell Biol. **2:**887–897.
19. **Gavard, J., M. Lambert, I. Grosheva, V. Marthiens, T. Irinopoulou, J.-F. Riou, A. Bershadsky, and R.-M. Mege.** 2003. Lamellipodium extension and cadherin adhesion: two cell responses to cadherin activation relying on distinct signaling pathways. J. Cell Sci. **117:**257–270.
20. **Govek, E.-E., S. E. Newey, C. J. Akerman, J. R. Cross, L. Van der Veken, and L. Van Aelst.** 2004. The X-linked mental retardation protein oligophrenin-1 is required for dendritic spine morphogenesis. Nat. Neurosci. **7:**364–372.
21. **Grunwald, I. C., M. Korte, G. Adelmann, A. Plueck, K. Kullander, R. H. Adams, M. Frotscher, T. Bonhoeffer, and R. Klein.** 2004. Hippocampal plasticity requires postsynaptic ephrinBs. Nat. Neurosci. **7:**33–40.
22. **Hahne, P., A. Sechi, S. Benesch, and J. V. Small.** 2001. Scar/WAVE is localized at the tips of protruding lamellipodia in living cells. FEBS Lett. **492:** 215–220.
23. **Henkemeyer, M., O. S. Itkis, M. Ngo, P. W. Hickmott, and I. M. Ethell.** 2003. Multiple Eph receptor tyrosine kinases shape dendritic spines in the hippocampus. J. Cell Biol. **163:**1313–1326.
24. **Hering, H., and M. Sheng.** 2001. Dendritic spines: structure, dynamics and regulation. Nat. Rev. Neurosci. **2:**880–888.
25. **Innocenti, M., P. Tenca, E. Frittoli, M. Faretta, A. Tocchetti, P. P. Di Fiore, and G. Scita.** 2002. Mechanisms through which Sos-1 coordinates the activation of Ras and Rac. J. Cell Biol. **156:**125–136.
26. **Innocenti, M., A. Zucconi, A. Disanza, E. Frittoli, L. B. Areces, A. Steffen, T. E. B. Stradal, P. P. Di Fiore, M.-F. Carlier, and G. Scita.** 2004. Abi1 is essential for the formation and activation of a WAVE2 signalling complex. Nat. Cell Biol. **6:**319–327.
27. **Irie, F., and Y. Yamaguchi.** 2002. Eph receptors regulate dendritic spine development via intersectin, Cdc42 and N-WASP. Nat. Neurosci. **5:**1117–1118.
28. **Juang, J. L., and F. M. Hoffmann.** 1999. Drosophila abelson interacting protein (dAbi) is a positive regulator of abelson tyrosine kinase activity. Oncogene **18:**5138–5147.
29. **Kobielak, A., H. A. Pasolli, and E. Fuchs.** 2004. Mammalian formin-1 participates in adherens junctions and polymerization of linear actin cables. Nat. Cell Biol. **6:**21–30.
30. **Kovacs, E. M., M. Goodwin, R. G. Ali, A. D. Paterson, and A. S. Yap.** 2002. Cadherin-directed actin assembly: E-cadherin physically associates with the Arp2/3 complex to direct actin assembly in nascent adhesive contacts. Curr. Biol. **12:**379–382.
31. **Kunda, P., G. Craig, V. Dominguez, and B. Baum.** 2003. Abi, Sra1, and Kette control the stability and localization of SCAR/WAVE to regulate the formation of actin-based protrusions. Curr. Biol. **13:**1867–1875.
32. **Lo, W. K.** 1988. Adherens junctions in the ocular lens of various species: ultrastructural analysis with an improved fixation. Cell Tissue Res. **254:** 31–40.
33. **Matus, A.** 2000. Actin-based plasticity in dendritic spines. Science **290:**754–758.
34. **McAvoy, J. W.** 1980. Induction of the eye lens. Differentiation **17:**137–149.
35. **Meng, Y., Y. Zhang, V. Tregoubov, C. Janus, L. Cruz, M. Jackson, W. Y. Lu, J. F. MacDonald, J. Y. Wang, D. L. Falls, and Z. Jia.** 2002. Abnormal spine morphology and enhanced LTP in LIMK-1 knockout mice. Neuron **35:** 121–133.
36. **Miyazaki, K., S. Matsuda, Y. Ichigotani, Y. Takenouchi, K. Hayashi, Y. Fukuda, Y. Nimura, and M. Hamaguchi.** 2000. Isolation and characterization of a novel human gene (NESH) which encodes a putative signaling molecule similar to e3B1 protein. Biochim. Biophys. Acta **1493:**237–241.
37. **Moresco, E. M., A. J. Scheetz, W. G. Bornmann, A. J. Koleske, and R. M. Fitzsimonds.** 2003. Abl family kinases modulate short-term synaptic plasticity. J. Neurophysiol. **89:**1678–1687.
38. **Morgenbesser, S. D., B. O. Williams, T. Jacks, and R. A. DePinho.** 1994. p53-dependent apoptosis produced by Rb-deficiency in the developing mouse lens. Nature **371:**72–74.
39. **Morgenbesser, S. D., N. Schreiber-Agus, M. Bidder, K. A. Mahon, P. A. Overbeek, J. Horner, and R. A. DePinho.** 1995. Contrasting roles for c-Myc and L-Myc in the regulation of cellular growth and differentiation in vivo. EMBO J. **14:**743–756.
40. **Murai, K. K., L. N. Nguyen, F. Irie, Y. Yamaguchi, and E. B. Pasquale.** 2003. Control of hippocampal dendritic spine morphology through ephrin-A3/EphA4 signaling. Nat. Neurosci. **6:**153–160.
41. **Nakayama, A. Y., M. B. Harms, and L. Luo.** 2000. Small GTPases Rac and Rho in the maintenance of dendritic spines and branches in hippocampal pyramidal neurons. J. Neurosci. **20:**5329–5338.
42. **Nishiguchi, S., H. Wood, H. Kondoh, R. Lovell-Badge, and V. Episkopou.** 1998. Sox1 directly regulates the gamma-crystallin genes and is essential for lens development in mice. Genes Dev. **12:**776–781.
43. **Penzes, P., A. Beeser, J. Chernoff, M. R. Schiller, B. A. Eipper, R. E. Mains, and R. L. Huganir.** 2003. Rapid induction of dendritic spine morphogenesis by trans-synaptic ephrinB-EphB receptor activation of the Rho-GEF kalirin. Neuron **37:**263–274.
44. **Piatigorsky, J.** 1981. Lens differentiation in vertebrates: a review of cellular and molecular features. Differentiation. **19:**134–153.
45. **Plattner, R., L. Kadlec, K. A. DeMali, A. Kazlauskas, and A. M. Pendergast.** 1999. c-Abl is activated by growth factors and Src family kinases and has a role in the cellular response to PDGF. Genes Dev. **13:**2400–2411.
46. **Ramakers, G. J. A.** 2002. Rho proteins, mental retardation and the cellular basis of cognition. Trends Neurosci. **25:**191–199.
47. **Reddy, B. A., M. Kloc, and L. D. Etkin.** 1992. The cloning and characterization of a localized maternal transcript in Xenopus laevis whose zygotic counterpart is detected in the CNS. Mech. Dev. **39:**143–150.
48. **Reya, T., A. W. Duncan, L. Ailles, J. Domen, D. C. Scherer, K. Willert, L. Hintz, R. Nusse, and I. L. Weissman.** 2003. A role for Wnt signaling in self-renewal of haematopoietic stem cells. Nature **423:**409–414.
49. **Ribar, T. J., R. M. Rodriguiz, L. Khiroug, W. C. Wetsel, G. J. Augustine, and A. R. Means.** 2000. Cerebellar defects in Ca^{2+}/calmodulin kinase IV-deficient mice. J. Neurosci. **20:**RC107.
50. **Rogers, S. L., U. Wiedemann, N. Stuurman, and R. D.Vale.** 2003. Molecular requirements for actin-based lamella formation in *Drosophila* S2 cells. J. Cell Biol. **162:**1079–1088.
51. **Sahai, E., and C. J. Marshall.** 2002. ROCK and Dia have opposing effects on adherens junctions downstream of Rho. Nat. Cell Biol. **4:**408–415.
52. **Schenck, A., B. Bardoni, A. Moro, C. Bagni, and J.-L. Mandel.** 2001. A highly conserved protein family interacting with the fragile X mental retardation protein (FMRP) and displaying selective interactions with FMRP-related proteins FXR1P and FXR2P. Proc. Natl. Acad. Sci. USA **98:**8844–8849.
53. **Schenck, A., B. Bardoni, C. Langmann, N. Harden, J. L. Mandel, and A. Giangrande.** 2003. CYFIP/Sra-1 controls neuronal connectivity in *Drosophila* and links the Rac1 GTPase pathway to the fragile X protein. Neuron **38:** 887–898.
54. **Schöck, F., and N. Perrimon.** 2002. Molecular mechanisms of epithelial morphogenesis. Annu. Rev. Cell. Dev. Biol. **18:**463–493.
55. **Schuz, A., and G. P. Demianenko.** 1995. Constancy and variability in cortical

structure. A study on synapses and dendritic spines in hedgehog and monkey. J. Hirnforsch. **36:**113–122.
56. **Scita, G., J. Nordstrom, R. Carbone, P. Tenca, G. Giardina, S. Gutkind, M. Bjarnegard, C. Betsholtz, and P. P. Di Fiore.** 1999. EPS8 and E3B1 transduce signals from Ras to Rac. Nature **401:**290–293.
57. **Scita, G., P. Tenca, L. B. Areces, A. Tocchetti, E. Frittoli, G. Giardina, I. Ponzanelli, P. Sini, M. Innocenti, and P. P. Di Fiore.** 2001. An effector region in Eps8 is responsible for the activation of the Rac-specific GEF activity of Sos-1 and for the proper localization of the Rac-based actin-polymerizing machine. J. Cell Biol. **154:**1031–1044.
58. **Shi, Y., K. Alin, and S. P. Goff.** 1995. Abl-interactor-1, a novel SH3 protein binding to the carboxy-terminal portion of the Abl protein, suppresses v-abl transforming activity. Genes Dev. **9:**2583–2597.
59. **Soderling, S. H., K. L. Binns, G. A. Wayman, S. M. Davee, S. H. Ong, T. Pawson, and J. D. Scott.** 2002. The WRP component of the WAVE-1 complex attenuates Rac-mediated signalling. Nat. Cell Biol. **4:**970–975.
60. **Soderling, S. H., L. K. Langeberg, J. A. Soderling, S. M. Davee, R. Simerly, J. Raber, and J. D. Scott.** 2003. Loss of WAVE-1 causes sensorimotor retardation and reduced learning and memory in mice. Proc. Natl. Acad. Sci. USA **100:**1723–1728.
61. **Soto, M. C., H. Qadota, K. Kasuya, M. Inoue, D. Tsuboi, C. C. Mello, and K. Kaibuchi.** 2002. The GEX-2 and GEX-3 proteins are required for tissue morphogenesis and cell migrations in *C. elegans.* Genes Dev. **16:**620–632.
62. **Steffen, A., K. Rottner, J. Ehinger, M. Innocenti, G. Scita, J. Wehland, and T. E. B. Stradal.** 2004. Sra-1 and Nap1 link Rac to actin assembly driving lamellipodia formation. EMBO J. **23:**749–759.
63. **Stradal, T., K. D. Courtney, K. Rottner, P. Hahne, J. V. Small, and A. M. Pendergast.** 2001. The Abl interactor proteins localize to sites of actin polymerization at the tips of lamellipodia and filopodia. Curr. Biol. **11:**891–895.
64. **Straub, B. K., J. Boda, C. Kuhn, M. Schnoelzer, U. Korf, T. Kempf, H. Spring, M. Hatzfeld, and W. W. Franke.** 2003. A novel cell-cell junction system: the *cortex adherens* mosaic of lens fiber cells. J. Cell Sci. **116:**4985–4995.
65. **Suetsugu, S., D. Yamazaki, S. Kurisu, and T. Takenawa.** 2003. Differential roles of WAVE1 and WAVE2 in dorsal and peripheral ruffle formation for fibroblast cell migration. Dev. Cell **5:**595–609.
66. **Svoboda, K., D. W. Tank, and W. Denk.** 1996. Direct measurement of coupling between dendritic spines and shafts. Science **272:**716–719.
67. **Tani, K., S. Sato, T. Sukezane, H. Kojima, H. Hirose, H. Hanafusa, and T. Shishido.** 2003. Abl interactor 1 promotes tyrosine 296 phosphorylation of mammalian enabled (Mena) by c-Abl kinase. J. Biol. Chem. **278:**21685–21692.
68. **Togashi, H., K. Abe, A. Mizoguchi, K. Takaoka, O. Chisaka, and M. Takeichi.** 2002. Cadherin regulates dendritic spine morphogenesis. Neuron **35:**77–89.
69. **Vasioukhin, V., C. Bauer, M. Yin, and E. Fuchs.** 2000. Directed actin polymerization is the driving force for epithelial cell-cell adhesion. Cell **100:**209–219.
70. **Vianna, M. R., L. A. Izquierdo, D. M. Barros, J. H. Medina, and I. Izquierdo.** 1999. Intrahippocampal infusion of an inhibitor of protein kinase A separates short- from long-term memory. Behav. Pharmacol. **10:**223–227.
71. **Wallar, B. J., and A. S. Alberts.** 2003. The formins: active scaffolds that remodel the cytoskeleton. Trends Cell Biol. **13:**435–446.
72. **Wang, B., T. Mysliwiec, D. Krainc, R. A. Jensen, G. Sonoda, J. R. Testa, E. A. Golemis, and G. D. Kruh.** 1996. Identification of ArgBP1, an Arg protein tyrosine kinase binding protein that is the human homologue of a CNS-specific Xenopus gene. Oncogene **12:**1921–1929.
73. **Welch, M. D., and R. D. Mullins.** 2002. Cellular control of actin nucleation. Annu. Rev. Cell. Dev. Biol. **18:**247–288.
74. **Westphal, R. S., S. H. Soderling, N. M. Alto, L. K. Langeberg, and J. D. Scott.** 2000. Scar/WAVE-1, a Wiskott-Aldrich syndrome protein, assembles an actin-associated multikinase scaffold. EMBO J. **19:**4589–4600.
75. **Yamamoto, A., T. Suzuki, and Y. Sakaki.** 2001. Isolation of hNap1BP which interacts with human Nap1 (NCKAP1) whose expression is down-regulated in Alzheimer's disease. Gene **271:**159–169.
76. **Yamazaki, D., S. Suetsugu, H. Miki, Y. Kataoka, S.-I. Nishikawa, T. Fujiwara, N. Yoshida, and T. Takenawa.** 2003. WAVE2 is required for directed cell migration and cardiovascular development. Nature **424:**452–456.
77. **Yap, A. S., and E. M. Kovacs.** 2003. Direct cadherin-activated cell signaling: a view from the plasma membrane. J. Cell Biol. **160:**11–16.
78. **Yu, X., and R. C. Malenka.** 2003. α-Catenin is critical for dendritic morphogenesis. Nat. Neurosci. **6:**1169–1177.
79. **Yuste, R., and T. Bonhoeffer.** 2001. Morphological changes in dendritic spines associated with long-term synaptic plasticity. Annu. Rev. Neurosci. **24:**1071–1089.
80. **Zhang, H., D. J. Webb, H. Asmussen, and A. F. Horwitz.** 2003. Synapse formation is regulated by the signaling adaptor GIT1. J. Cell Biol. **161:**131–142.
81. **Zhang, P., C. Wong, R. A. DePinho, J. W. Harper, and S. J. Elledge.** 1998. Cooperation between the Cdk inhibitors p27(KIP1) and p57(KIP2) in the control of tissue growth and development. Genes Dev. **12:**3162–3167.
82. **Ziemnicka-Kotula, D., J. Xu, H. Gu, A. Potempska, K. S. Kim, E. C. Jenkins, E. Trenkner, and L. Kotula.** 1998. Identification of a candidate human spectrin Src homology 3 domain-binding protein suggests a general mechanism of association of tyrosine kinases with the spectrin-based membrane skeleton. J. Biol. Chem. **273:**13681–13692.